Insulin Secretory Granules Release Exosomal miR-503 to Promote Insulin Resistance and β-Cell Senescence

Xiao Han (hanxiao@njmu.edu.cn)
Nanjing Medical University https://orcid.org/0000-0002-6467-1802
Yuncai Zhou
Nanjing Medical University
Kerong Liu
Nanjing Medical University
Yi Sun
Nanjing Medical University
Yan Zhang
Nanjing Medical University
Yangyang Wu
Nanjing Medical University
Ying Shi
Nanjing Medical University
Zhengjian Yao
Nanjing Medical University
Yating Li
Nanjing Medical University
Rongjie Bai
Nanjing Medical University
Rui Liang
Nankai University
Peng Sun
Nanjing Medical University
Xiaoai Chang
Nanjing Medical University
Wei Tang
Nanjing Medical University
Shuseng Wang
Nankai University
Yunxia Zhu

Nanjing Medical University https://orcid.org/0000-0002-4597-4445

Article

Keywords: Insulin secretory granules, Exosomal miR-503, Insulin Resistance, β-Cell Senescence

Posted Date: September 9th, 2020

DOI: https://doi.org/10.21203/rs.3.rs-58542/v1

Insulin Secretory Granules Release Exosomal *miR-503* to Promote Insulin Resistance and β-Cell Senescence

Yuncai Zhou,[1,4] Kerong Liu, [1,4] Yi Sun,[1,4] Yan Zhang,[1] Yangyang Wu[1], Ying Shi,[1] Zhengjian Yao,[1] Yating Li,[1] Rongjie Bai,[1] Rui Liang,[2] Peng Sun,[1] Xiaoai Chang,[1] Wei Tang,[3] Shusen Wang,[2] Yunxia Zhu,[1,*] and Xiao Han[1,5,*]

[1]Key Laboratory of Human Functional Genomics of Jiangsu Province, Nanjing medical University, Nanjing, Jiangsu 211166, China

[2]Organ Transplant Center, Tianjin First Central Hospital, Nankai University, Tianjin 300192, China

[3]Department of Endocrinology, Geriatric Hospital of Nanjing Medical University, Nanjing, Jiangsu 210024, China

[4]These authors contributed equally

[5]Lead contact

*Correspondence: zhuyx@njmu.edu.cn; hanxiao@njmu.edu.cn

Abstract

Chronic inflammation promotes pancreatic β-cell decompensation to insulin resistance due to local accumulation of supraphysiologic IL-1β levels. However, the underlying molecular mechanism(s) remains elusive. We show that *miR-503*, exclusively induced in islets from type 2 diabetic humans and rodents, is specifically upregulated by IL-1β in β cells. β-cell–specific *miR-503* transgenic (*miR-503*TG) mice display expression-dependent mild diabetes, severe diabetes, and premature death due to inflammation-induced multiple organ failure. By contrast, deletion of the *miR-503* cluster protects mice from high-fat-diet–induced insulin resistance. Single-cell RNA sequencing indicates infiltration of immune cells and senescent β cells in *miR-503*TG islets. Exosomes containing *miR-503* localize in insulin granules of senescent β cells. Autocrine *miR-503* activates MAPKs to inhibit β-cell function and replication. Telecrine *miR-503* targets *Insr/Igf1r* to dampen insulin signals in liver and adipose tissues. A metaflammation-related and inflammaging-related *miR-503* expression may therefore induce type 2 diabetes via insulin resistance and β-cell dysfunction.

Introduction

Type 2 diabetes mellitus (T2DM) is a metabolic disorder characterized by chronic hyperglycemia due to absolute or relative insulin insufficiency. Secretion of insulin by pancreatic β cells is highly regulated with feeding activities. Upon secretion, insulin binds to insulin receptors (INSR) and activates the PI3K/AKT signaling pathway to maintain postprandial glucose homeostasis[1]. The insulin signaling cascade inhibits hepatic glucose production (HGP), stimulates glucose uptake in the adipose tissue and skeletal muscle, and promotes the conversion of glucose into fat and glycogen for energy storage. Defects in insulin action and secretion, referring to insulin resistance and β-cell dysfunction, can give rise to insulin signaling disturbances and reciprocally promote diabetes progression[2]. However, these defects co-exist in the majority of T2DM patients, so no concerted insights have yet been reached regarding the cause-and-effect links between them.

Insulin resistance can persist for many years before the appearance of frank diabetes, and β cells can adapt to insulin resistance via insulin hypersecretion[3]. However, β-cell compensation can degenerate to decompensation in response to islet inflammation and the resulting production of proinflammatory factors, principally interleukin (IL)-1β[4]. The β cells are especially vulnerable to IL-1β, as the IL-1 receptor is one of the most abundantly expressed cell-surface receptors on β cells[5]. For this reason, anti-IL-1β approaches have been studied and have shown reduced tissue inflammation and anti-diabetic effects in rodents[6]. Unfortunately, in the clinical setting, the protective effects only manifest as improved β-cell function in T2DM patients, suggesting that the long-term hyperglycemia phenotype may not exclusively involve insulin insufficiency[7]. Instead, compensatory remodeling of the β-cell mass and function may initiate other epigenetic processes that cannot be disrupted by interrupting IL-1β signaling. Indeed, epigenetic cues, such as DNA methylation, histone modification, and noncoding RNAs (ncRNAs), have comprehensive impacts on the remodeling of metabolically stressed β cells in the context of chronic inflammation[8,9].

One subset of ncRNAs of particular interest in terms of diabetes, inflammation, and aging-related disorders are the microRNAs (miRNAs). These are endogenous small ncRNAs (~22 nucleotides) that play important roles in virtually all aspects of biological processes, and their dysregulation has been implicated in the pathogenesis of various diseases[10]. The miRNAs are transcribed as primary miRNAs (pri-miRNAs), which undergo a two-step cleavage by the endoribonucleases Drosha and Dicer to form the mature miRNA. The mature miRNA assembles into the RNA-induced silencing complex (RISC) and

activates the complex, which then targets mRNA for translational inhibition and/or mRNA degradation[11].

Numerous studies have demonstrated that miRNAs can be delivered into the bloodstream, and that they act as hormone-like molecules to facilitate crosstalk among key metabolic organs under obesity and diabetes conditions. The inter-organ and intra-organ communications confirm that miRNAs can also function as physiological ligands for certain RNA receptors, such as murine Toll-like receptor 7 (TLR7) and human TLR8[12]. One miRNA, the prototypical *miR-29*, is considered a gene regulator, a ligand of TLR7, and a modulator of metabolic organs in the context of T2DM[13,14]. We have discovered that *miR-29* exosomes derived from β cells are regulated by IL-1β and promote the development of diabetes by facilitating monocyte/macrophage activation. However, an elevation of *miR-29* is observed in almost all metabolic tissues, so whether IL-1β regulates the β-cell–dominant miRNA(s) linking islet inflammation to the development of T2DM requires further investigation.

In the present study, we identified *miR-503* as a master regulator of β-cell decompensation in IL-1β–induced islet inflammation. Moreover, *miR-503* was located within insulin secretory granules and underwent release as exosomes, an exclusive phenomenon observed in β cells. The release of exosomal *miR-503* triggered insulin resistance and β-cell dysfunction in both telecrine and autocrine manners. The X-linked *miR-503* is clustered with *miR-424*(*322*) and serves as an intracellular gene regulator to modulate fundamental processes that include cell proliferation, cell differentiation, and tissue remodeling[15]. Our investigation identified a previously unappreciated role of *miR-503* as an intra- and inter-organ modulator and defined its contribution to the development of type 2 diabetes using gain-of-function and loss-of-function genetic mouse models, as well as primary human islets.

Results

Promoter hypomethylation permits *miR-503* expression in β cells under inflammation and diabetes conditions. The miRNAs that could mimic the effects of IL-1β were revealed by miRNA microarray screening and cell viability comparisons. We identified *miR-503* as one of the six most upregulated miRNAs in β cells after treatment with IL-1β (Supplementary Fig. 1a, 1b). We confirmed *miR-503* upregulation by IL-1β in mouse islets, human islets, and INS-1 cells (Fig. 1a, 1b; Supplementary Fig. 1c).

The six altered miRNAs were overexpressed INS-1 cells for 24 h and the overexpressing cells were treated with a high dose of IL-1β for another 24 h. Cell viabilities were significantly inhibited by

expression of *miR-25*, *miR-146a*, *miR-503*, and *miR-153*, but cells transfected with *miR-146a* and *miR-503* showed no further decrease in cell viability after IL-1β administration (Supplementary Fig. 1d). This finding suggested that these two miRNAs were able to mimic IL-1β effects or that they might function as downstream effectors. Some reports have shown that *miR-146* expression was strongly increased by IL-1β and could suppress IL-1β effects by targeting *IRAK1* and *Traf6*, thereby diminishing MAPK and NF-κB signal transduction[16]. Lynn et al. reported that *miR-503* is enriched in E14.5 pancreases and is necessary for pancreas organogenesis[17]. In the present study, *miR-503* was enriched in embryo pancreata, but its expression was significantly decreased postnatally and was maintained at a relatively low level in adult islets and β cells (Supplementary Fig. 1e -1g). However, the expression of mature *miR-503* was significantly increased in primary islets from diabetic GK rats, *db*/*db* mice, high fat diet (HFD)-fed mice, 2-year-old aged mice, and type 1 diabetic NOD mice (Fig. 1c-1f; Supplementary Fig. 1h-1l). The serum *miR-503* levels were also elevated in diabetic mice (Fig. 1g, 1h; Supplementary Fig. 1m).

The metabolic organ that contributed to the increased *miR-503* level in the sera under diabetes condition was determined by examining transcripts of *miR-503* (*pri-miR-503*) in HFD-fed mice as well as in aged mice. The levels of *pri-miR-503* increased slightly in muscle and white adipose tissue (WAT), but *pri-miR-503* expression increased more than 40-fold in HFD-fed mouse islets and about 10-fold in aged mouse islets (Fig. 1i, 1j). Therefore, the pancreatic islets, or more specifically the β cells, might release *miR-503* into the circulatory system.

DNA methylation is frequently involved in gene silencing and re-expression during development and under disease conditions[18]. Analysis of the promoter region of *miR503HG* revealed extensive CpG sites in region -3617 bp ~ -1417 bp in both human and mouse genomes (Fig. 1k). A search of the human genome methylation database, based on the Illumina HumanMethylation450 BeadChip of more than 300 subjects, showed hypomethylation of this region of *miR503HG* in patients with type 2 diabetes (http://bio-bigdata.hrbmu.edu.cn/diseasemeth/) (Fig. 1l). Treatment with the DNA methylation inhibitor 5-azacytidine (5-Aza) significantly induced miR-503 transcripts in both primary human islets and MIN6 cells (Fig. 1m, 1n). Trichostatin A (TSA), a histone deacetylase inhibitor, also induced *miR-503* expression, but inhibition of DNA methylation had a much stronger regulatory effect on *miR-503* transcription (Supplementary Fig. 1n). The expression of *pri-miR-503* was significantly increased in primary islets from human diabetic patients (Fig. 1o), and a pancreas-associated *miR-503*, which is

silent in adult β cells, is re-expressed under inflammatory and diabetic conditions due to hypomethylation of the promoter region -3617 bp ~ -1417 bp. This regulatory process is conserved from rodents to humans.

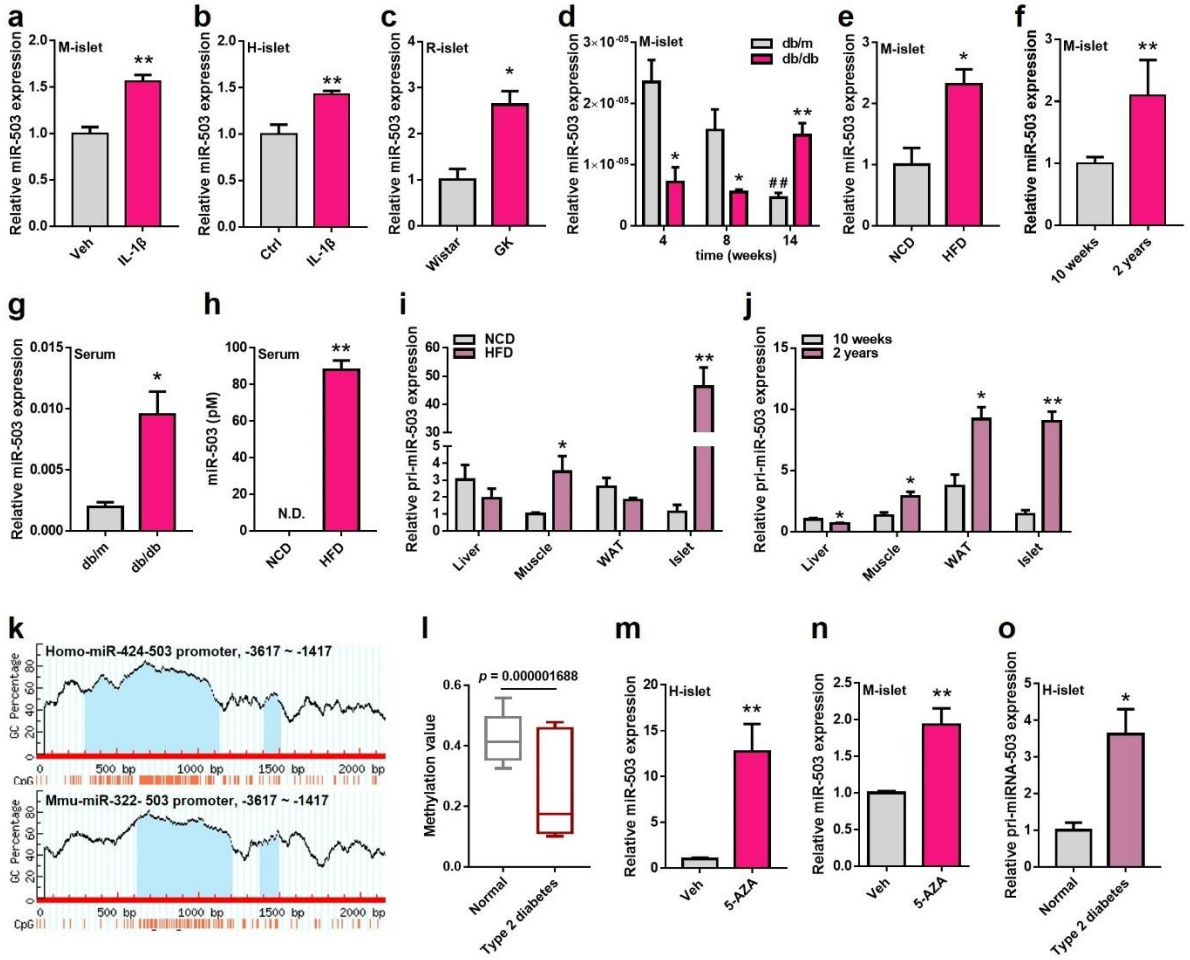

Fig. 1 Promoter hypomethylation permits *miR-503* expression in β cells under inflammation and diabetes conditions. **a, b** *MiR-503* expression in primary islets treated with 10 ng/ml IL-1β for 24 h was measured by qPCR: mice (**a**) or human (**b**) islets. **c-f** qPCR assays showing *miR-503* expression in diabetic murine islets: GK rats (**c**), different aged *db/db* mice (**d**), 4-month HFD fed C57/BL6J mice (**e**), 2-year-old C57/BL6J mice (**f**). **g, h** *MiR-503* contents in mice serum by using relative qPCR assay in 14-week-old db/db mice (**g**) or by absolute qPCR assay in 4-month HFD fed C57/BL6J mice (**h**). **i, j** qPCR analysis of *miR-503* transcription level represented by *pri-miR-503* expression of 4-month HFD fed (**i**) and 2-year-old C57/BL6J mice (**j**) tissue. **k** CpG island analysis of *miR-503HG* promoter region separately in human (up) and mice (down) by using MethPrimer program. **l** DNA methylation analysis of *miR-503HG* promoter in T2D patients in accordance with DiseaseMeth database. **m, n** Human (**m**) and mice (**n**) islets were treated with 10 μmol/l 5-AZA for 24 h, and miR-503 expression was quantified by using qPCR assay. **o** qPCR analysis of *miR-503* transcription level represented by *pri-miR-503* expression in islets from healthy or T2D patients. Bar graph data are presented as mean ±SEM, *p < 0.05, **p < 0.01, t test, n ≥ 3 per group.

Transgenic overexpression of *miR-503* in beta cells promotes diabetes and lethality. *miR-503* is one of the clustered miRNAs that is polycistronically expressed with *miR-322* (human *miR-424*) and *miR-351*. We studied the in vivo role of this cluster in the development of diabetes by constructing a

transgenic mouse expressing a β-cell specific *miR-503-322-351* cluster driven by the rat Ins2 promoter (Cluster TG) (Supplementary Fig. 2a, 2b). Analysis of the phenotype of 12 F1 pups with copy numbers of ~25 from two different founder mice (Supplementary Fig. 2c) revealed that the Cluster TG mice were weak and defective in growth because of severe hyperglycemia (Supplementary Fig. 2d - 2f). Insulin intervention had no effect on lowering the blood glucose levels of the Cluster TG pups, and the F1 pups were unable to survive longer than 34 days (Supplementary Fig. 2g). H&E staining showed a significantly decreased islet mass in the Cluster TG mice due to a defect in β-cell replication and a β-to-α cell transdifferentiation (Supplementary Fig. 2h - 2m). Thus, *miR-503-322-351* overexpression in β cells resulted in growth defects, severe diabetes, and lethality at an early age due to a significant loss of β-cell numbers.

We conducted a further investigation of the role of *miR-503* in β cells and disease progression by constructing *miR-503* transgenic mice with the rat Ins2 promoter (*miR-503*TG) and using our knowledge that the flanking sequences are critical for miRNA maturation[19]. To ensure overexpression of *miR-503*, 300 bp of both upstream and downstream sequences were included in the construct and the full sequence of *miR-322* was involved. We preserved three lines of *miR-503*TG mice with different copy numbers of *miR-503*: Line50 (5.2), Line58 (13.3), and Line57 (22.9) (Fig. 2a and 2b). The increase in *miR-503* in islets was copy number dependent (Fig. 2c). No elevation of *miR-322* was observed in islets (data not shown). Therefore, three genetically stable lines of β-cell specific miR-503 overexpressing mice were obtained.

The newborn mice were normal, but Line58 and Line57 mice started to lose weight at four weeks. The differences in body weight increased further due to a deficiency in fat production (Fig. 2d, 2e). The random blood glucose (RBG) levels of *miR-503*TG mice increased in parallel with *miR-503* expression (Fig. 2f). Line58 mice were dramatically glucose intolerant at six weeks (Fig. 2g). No alterations in fasting insulin levels were observed, but insulin and C-peptide levels were significantly decreased after refeeding (Fig. 2h, 2i). Metabolic cage experiments using Line50 and Line58 mice did not reveal any obvious alterations in Line50 mice at seven weeks, whereas the Line58 mice showed a decreased respiratory exchange ratio (RER) during the night (Fig. 2j), suggesting that the Line58 mice preferred to use fat as an energy source. Feeding behavior showed no differences between the groups; however, the daily food intake and water consumption were significantly greater in the Line58 mice (Fig. 2k, 2l). Body composition analysis showed no effect on lean mass but a significant decrease in fat mass in

Line58 mice. The amount of epididymal white adipose tissue (eWAT) was smaller in Line58 mice than in their WT littermates due to defective adipocyte differentiation (Fig. 2m - 2o; Supplementary Fig. 3a).

Serum insulin levels varied in the fasted state (Supplementary Fig. 3b), and HOMA-IR analysis according to the fasting blood glucose and serum insulin levels of each mouse confirmed a severe insulin resistance in the *miR-503*TG mice (Fig. 2p, 2q). Like Cluster TG mice, Line57 mice could not survive for more than ten weeks (Fig. 2r). Careful dissection of the mice showed that most of the jejunum and ileum had turned black because of hemorrhage and necrosis (Fig. 2s). The serum characteristics of the Line57 mice indicated severe hepatic failure and renal dysfunction (Fig. 2t - 2v; Supplementary Fig. 3c - 3e). Collectively, the results from the Cluster TG and *miR-503*TG mice strongly supported that overexpression of *miR-503* in β cells cause severe insulin resistance, defective refed insulin secretion, advanced diabetes, multiple organ failure, and early lethality.

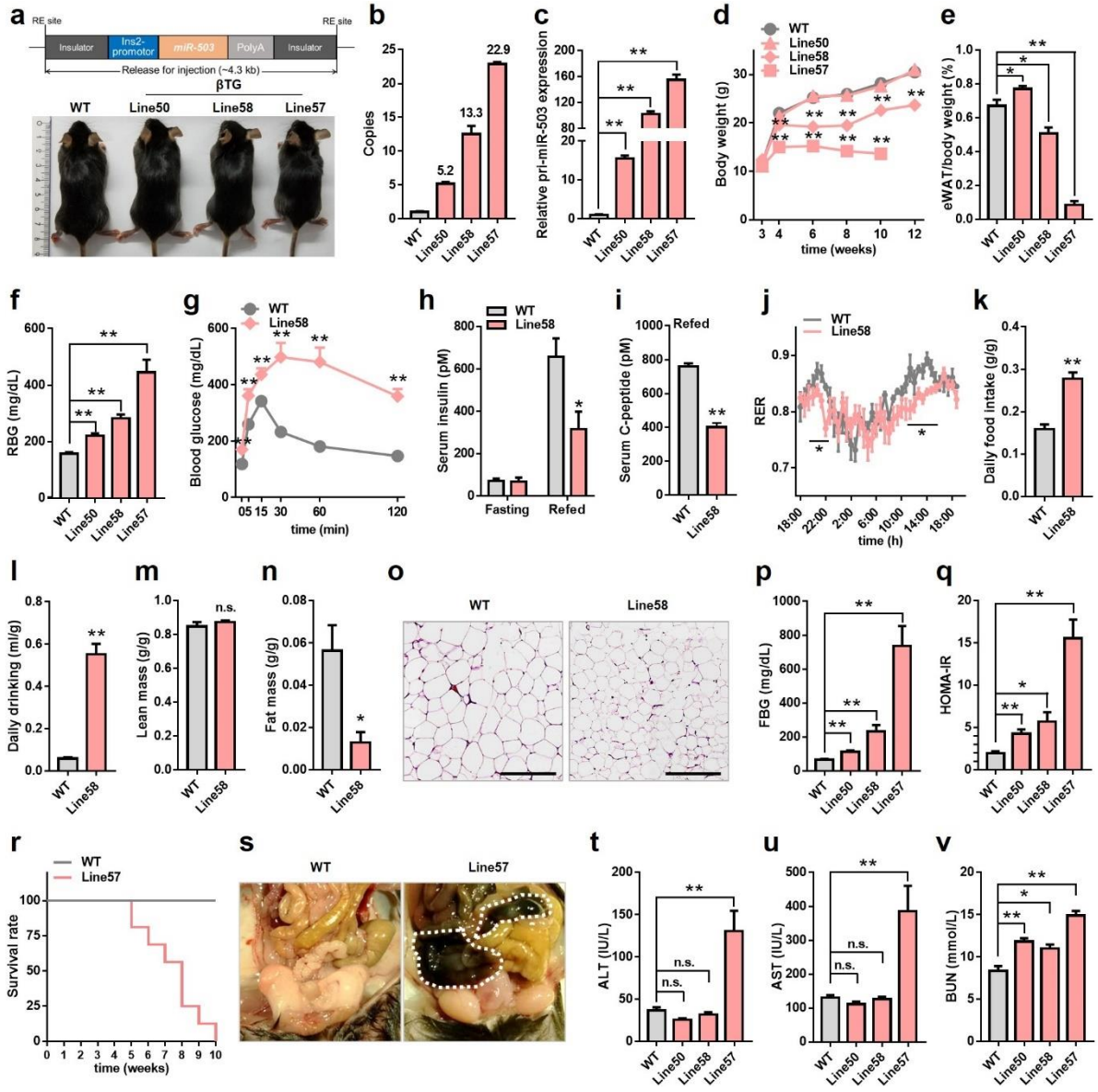

Fig. 2 β-cell transgenic overexpressed *miR-503* promotes diabetes and lethality. **a** The schematic of recombinant plasmid used for β cell specific transgenic *miR-503* mice construction and whole-mount image. **b-f** Gene copies (**b**), *miR-503* expression (**c**), body weight accompanies with age (**d**), percentage of white adipose tissue in body weight (**e**), and plasma glucose level of randomly fed three βTG line mice and their littermates (**f**). **g-i** IPGTT (**g**), serum insulin (**h**) and c-peptide (**i**) level of 6-week-old Line58 mice. **j-o** Daily respiratory exchange rate (**j**), daily food intake (**k**), daily drinking (**l**), lean mass (**m**), fat mass (**n**) and adipose tissue section (**o**) of 10-week-old Line58 mice and their littermates. **p, q** Fasted blood glucose and HOMA-IR of 6-week-old three βTG line mice and their littermates. **r ,s** Survival rate (**r**) and lower abdomen image (**s**) of Line57 and WT mice. (**t-v**) Glutamic-pyruvic transaminase (**t**), glutamic oxalacetic transaminase (**u**), and blood urea nitrogen (**v**) level in 10-week-old mice serum. Error bars represent the SEM, N.S. means not significant, *p < 0.05, **p < 0.01, t test, n ≥ 3 per group.

Metabolic stress enhances *miR-503*-induced insulin resistance and glucose intolerance. Aging and overnutrition are two metabolic stresses common to both human and rodents. The *miR-503* expression level in islets from Line50 mice resembled those of aged mice and HFD-fed mice. Therefore, Line50 mice were subjected to constant evaluation with age under both normal chow diet (NCD) and

HFD feeding conditions. Glucose intolerance in the Line50 mice manifested at 8 weeks (Fig. 3a, 3b), but in vivo glucose-stimulated insulin secretion (GSIS) was enhanced in Line50 mice over that in WT mice (Fig. 3c), ruling out an involvement of defective insulin secretion. Prolonged elevation of *miR-503* strengthened the glucose intolerance of Line50 mice due to severe insulin resistance, since no alterations in serum insulin level were observed (Fig. 3d, 3e; Supplementary Fig. 4a, 4b).

HFD feeding causes hyperinsulinemia to augment insulin resistance, and mice manifest hyperglycemia due to β-cell failure. Here, Line50 mice showed impaired glucose tolerance, insulin insensitivity, and no alterations of body weight when compared with WT mice fed on a HFD (Fig. 3f, 3g; Supplementary Fig. 4c). The between-group differences in insulin insensitivity were less apparent in HFD-fed than in NCD-fed mice (Fig. 3e, 3g). The diminished in vivo GSIS function of Line50 mice might be associated with this lessened effect (Fig. 3h).

We ascertained the exact tissues involved in insulin resistance in 16-week-old mice fed a NCD by performing a standard hyperinsulinemia-euglycemic clamp technique using [3-^{3}H]-glucose and 2-deoxy-D-[1-^{14}C]-glucose as tracers (Fig. 3i). After constant insulin infusion, the blood glucose levels of both groups were clamped at similar levels (Fig. 3j). The glucose infusion rate (GIR) tended to decrease in Line50 mice compared with WT mice, and the steady GIR was significantly lower in Line50 mice than in WT mice (Fig. 3k, 3l), in accordance with the changes observed in glucose tolerance test (GTT) results. The whole-body use of glucose and the clamped glucose disposal rate (GDR) were defective in Line50 mice due to insufficient glucose uptake in the adipose tissue but not in the muscle and liver (Fig. 3m - 3p; Supplementary Fig. 4d, 4e). Basal hepatic glucose production (HGP) was not altered in Line50 mice, whereas insulin-inhibited HGP was significantly diminished (Supplementary Fig. 4f, 3q). No alterations were noted in glycogen synthesis in liver and skeletal muscle (Supplementary Fig. 4g, 4h). Whole body lipogenesis was also unchanged, in line with the similar body weight observed between groups (Supplementary Fig. 4i). Taken together, these results demonstrated that both physiological (age) and pathological (feeding behavior) metabolic stresses enhanced the diabetic phenotype of the *miR-503*TG mice. At an early stage, *miR-503*TG mice showed hyperinsulinemia, insulin resistance, and glucose intolerance, and HFD feeding caused the *miR-503*TG mice to fail to secrete sufficient insulin, thereby worsening their glucose intolerance.

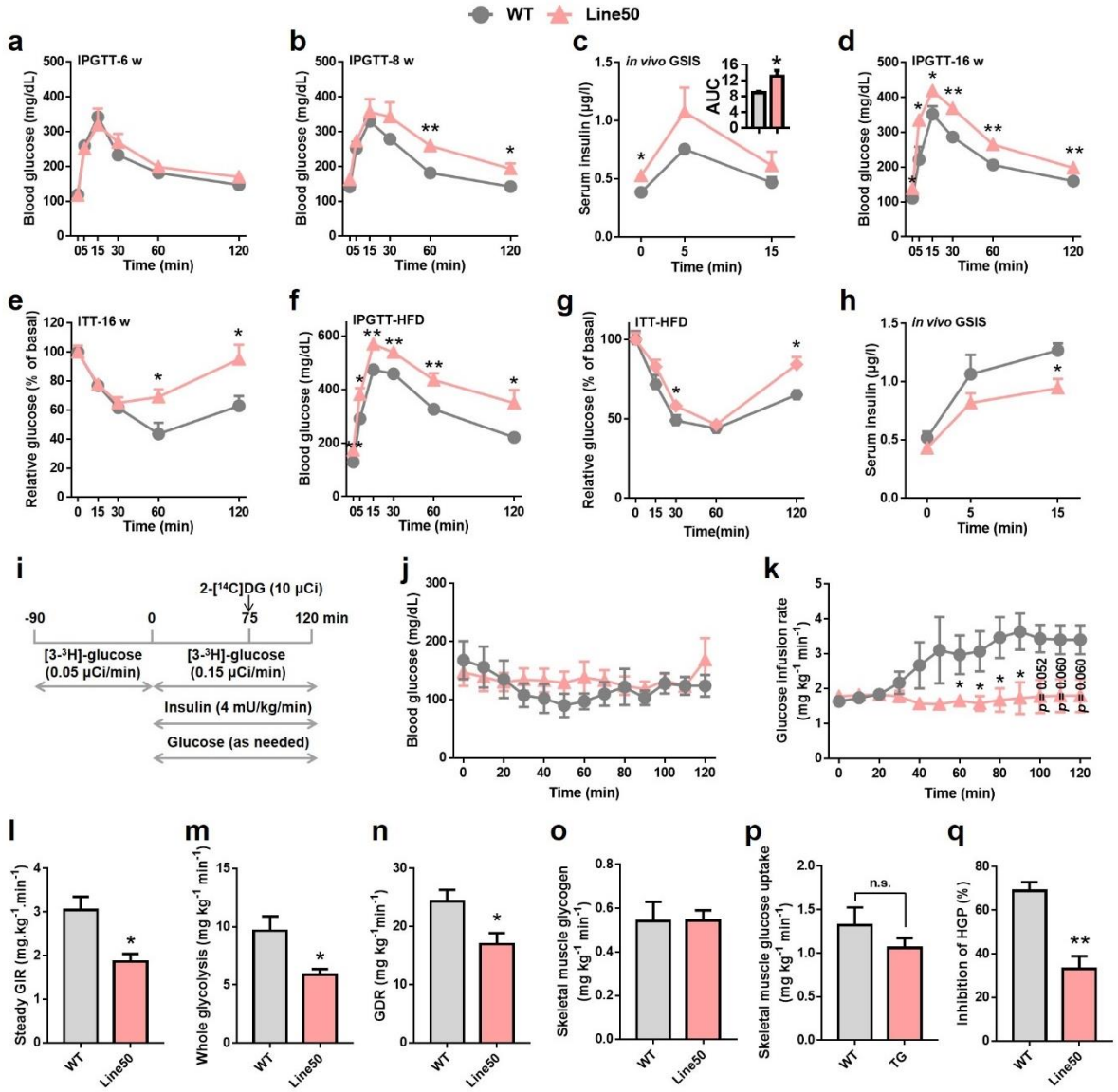

Fig. 3 Metabolic stress enhances *miR-503* induced insulin resistance and glucose intolerance. **a-e** IPGTT (**a, b** and **d**), in vivo GSIS (**c**), IPITT (**e**) of randomly fed Line50 mice and their littermates. Mice at the age of 6 weeks(**a**), 8 weeks (**b, c**), 16 weeks (**d, e**). **f-h** IPGTT (**f**), IPITT (**g**), and in vivo GSIS (**h**) of 2-month HFD fed Line50 and WT mice. **i-q** Hyperinsulinemic-euglycemic clamp assay of 16-week-old WT and Line50 mice, protocol (**i**), blood glucose levels (**j**), glucose infusion rate (**k**), statistical analysis of GIR (**l**), whole body glycolysis (**m**), rate of glucose disposal (**n**), adipose tissue glucose uptake (**o**), skeletal muscle glucose uptake (**p**) and inhibition of hepatic glucose production (**q**). Error bars represent the SEM, *p < 0.05, **p < 0.01, t test, n ≥ 3 per group.

ScRNA-Seq identifies immune-cell infiltration and β-cell senescence in *miR-503*TG islets. The role of *miR-503* in pancreatic islet cells was further studied by single-cell RNA sequencing (scRNA-Seq) in primary islets from 10-week-old mice. Overall, 8,698 qualified islet cells, either from WT or Line50 mice, were processed for transcriptomic analysis. The cells were projected onto a two-dimensional t-distributed stochastic neighbor embedding (tSNE) plot and then analyzed by two different methods, Graph-based and K-means, to cluster the cells according to their expression similarities. Only

endotheliocytes and macrophages were identified by marker genes using the Graph-based algorithm. whereas adjusting the K value to six clearly distinguished marker gene clustering for two clusters of β cells, α/δ/PP cells, endotheliocytes, immune cells, and β-cell resident macrophages (BRM) (Fig. 4a, 4b). The cell types between WT and Line50 islets were barely distinguishable; however, cell distributions were significantly changed (Fig. 4c). A decrease in β cells and increases in α cells and PP cells, but no alteration in δ cells, were confirmed by cross-immunostaining for glucagon, polypeptide, and somatostatin with insulin (Supplementary Fig. 5a - 5e). Dramatically decreased numbers of endotheliocytes were in line with the smaller islet size of *miR-503*TG mice. A slight decrease in BRM was observed, but considerable numbers of *Ccr6/Ccr7* positive immune cells had infiltrated the *miR-503*TG islets (Fig. 4c), suggesting a remodeling of the immune environment in the *miR-503* overexpressing β cells.

Some reports have shown that β cells are heterogeneous and can be divided into different subpopulations by functional means[20]. We examined the β-cell fate determined by *miR-503* by adjusting the K value to reveal the diverse subpopulations of β cells. Differential gene expression in β cells trended to cluster the cells into three subtypes, β1, β2 and β3 cells, when the K value was adjusted to 9 (Supplementary Fig. 5f, 5g). A trajectory analysis, used to derive the pseudotime of the β cells in a continuous process, revealed pseudotime ordering of β-cell maturation from right to left and a trajectory consisting of seven decision points (Fig. 4d). The three cell subtypes were named by their feature genes as β3: high *Gast*-low *Hba* ($Gast^{hi}Hba^{lo}$), β1: low *Gast*-low *Hba* ($Gast^{lo}Hba^{lo}$), and β2: low *Gast*-high *Hba* ($Gast^{lo}Hba^{hi}$) which corresponded to three major β-cell states of β1 (GSIS functional β cells), β2 (senescent β cells), and β3 (proliferative β cells) (Supplementary Fig. 5h - 5j). Overexpression of *miR-503* reduced the numbers of both the proliferative and functional β cells but significantly augmented the numbers of senescent β cells (Fig. 4f). Numerous markers unique for β-cell senescence were identified in the senescent subtype (Fig. 4g). Expressions of these marker genes were conformed in primary islets from 2-year-old aged mice and some of these markers were also increased in HFD islets (Supplementary Fig. 5k, 5l). Therefore, we demonstrated, from a single-cell perspective, that overexpression of *miR-503* in β cells can attract circulatory immune cells to islets and accelerate β-cell senescence. Both of these responses would jeopardize GSIS function.

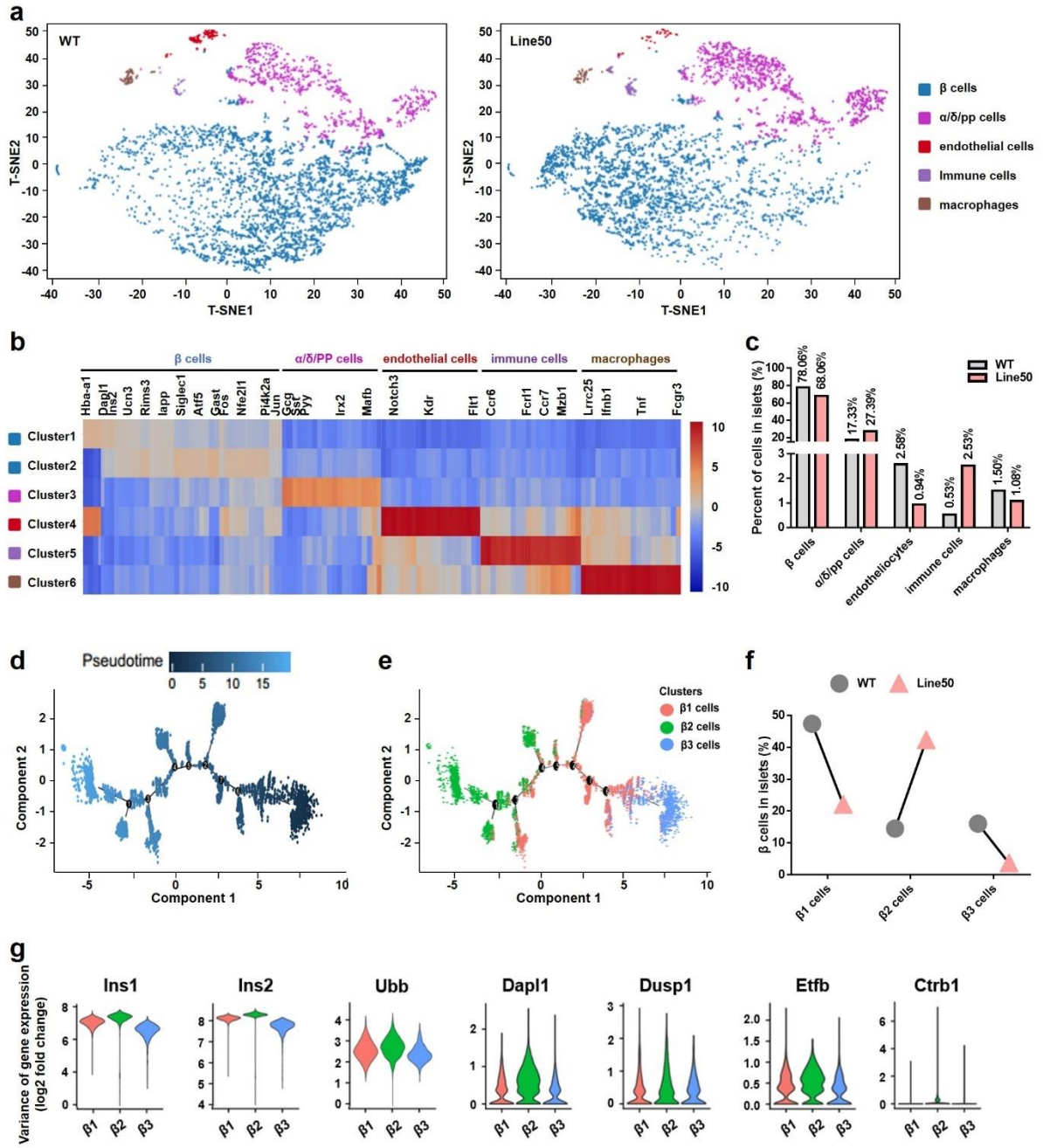

Fig. 4 ScRNA-Seq Identifies Immune-Cell Infiltration and β-Cell Senescence in *miR-503*TG islets. **a-g** Analysis of scRNA-sequence of islets from 10-week-old WT and Line50 mice, tSNE plots (**a**), heatmap of all cells clustered by K-means = 5 clustering, showing selected marker genes for every population (**b**), percentage of each cell clusters in islets from WT or Line50 mice separately (**c**), maturation trajectory (**d**) and distribution (**e**) of three subtype β cells constructed by Monocle, percentage of different subtype β cells from different mice respectively (**f**), specific senescence associated genes across sub-clusters demonstrated by violin plots (**g**). Cell types are represented by colors.

***MiR-503*, akin to IL-1β, causes β-cell defects by activating the MAPK and NF-κB pathways.** Some reports have shown that the physiological concentration of IL-1β increases insulin secretion, whereas higher levels inhibit GSIS function, insulin biosynthesis, and cell viability[21,22]. A further investigation of

the effects of *miR-503* and IL-1β in β cells, human islets, mouse islets, and MIN6 cells revealed that *miR-503* expression could increase K^+-induced insulin secretion, reduce insulin levels, and suppress GSIS function in β cell lines, thereby mimicking both the physiological and pathological effects of IL-1β (Fig. 5a - 5c). Both a stimulatory effect and an inhibitory effect of *miR-503* on insulin secretion were confirmed in perfused human islets (Fig. 5d, 5e; Supplementary Fig. 6a). Mouse islets from *miR-503*TG mice also exhibited an increased release of basal insulin and a decreased release of glucose-potentiated insulin due to the glucose insensitivity of the *miR-503*-overexpressing β cells (Fig. 5f, 5g). Aged islets of Line50 mice showed both first-phase and second-phase deficiencies (Supplementary Fig. 6b, 6c). Although serum insulin levels were barely affected by *miR-503* expression in Line50 mice, the insulin content of the whole pancreas was significantly diminished (Fig. 5h). By contrast, transcripts of *Ins1* and *Ins2* were upregulated in Line50 islets (Fig. 5i, 5j), suggesting that *miR-503* promoted in vivo insulin secretion and gene transcription.

The changes in subcellular structures were monitored by transmission electron microscopy (TEM) analysis of primary islets from WT and Line50 mice. IL-1β caused β-cell defects by activating ER stress and oxidative stress, as indicated by ER dilation and mitochondrial swelling. The same abnormities in the ER and mitochondria were also evident in *miR-503*-overexpressing β cells (Fig. 5k). The numbers of immature insulin granules (ISG) substantially increased and assumed a location near the cell membrane, so that the numbers of secretory granules remained unchanged (Fig. 5k - 5m).

In addition to its involvement in function, *miR-503* expression also influenced β-cell mass under NCD-fed and HFD-fed conditions. The islet size was smaller in Line50 mice than in WT mice because of a suppression of β-cell replication caused by *miR-503* (Fig. 5n - 5r). These discrepancies in islet size reduction were amplified by HFD feeding and by the number of *miR-503* insertion copies (Fig. 5o - 5r, Supplementary Fig. 6d, 6e). No apoptotic cells were observed in *miR-503*-overexpressing islets (Supplementary Fig. 6f). Therefore, *miR-503* appeared to act as a brake in the compensatory proliferation of β cells induced by the HFD.

IL-1β engages the MAPK and NF-κB pathways to transduce signaling. Luciferase reporter gene assays based on activities of transcriptional factor AP-1 and NF-κB revealed that *miR-503* significantly enhanced AP-1 and NF-κB activities. However, this response was partially blocked by IL-1RA, an antagonist of IL-1R1 (Supplementary Fig. 6g, 6h), suggesting that *miR-503* might compete with IL-1β for IL-1 receptors. We verified this possibility by transfecting Cy3-labled *miR-503* into β cells, and we

clearly observed a cell membrane distribution of *miR-503* in MIN6 cells (Supplementary Fig. 5s). Moreover, IL-1R was largely co-localized with *miR-503* in a vesicle structure (Supplementary Fig. 6i). The phosphorylation levels of P38 MAPK and JNK MAPK were strongly boosted, whereas ERK MAPK was significantly inhibited by *miR-503* expression (Fig. 5t). Taken together, these results show that *miR-503* substitutes for IL-1β to evoke MAPKs and NF-κB signaling transduction, coupled with β-cell compensatory insulin secretion, to promote β-cell decompensation under metabolic stress.

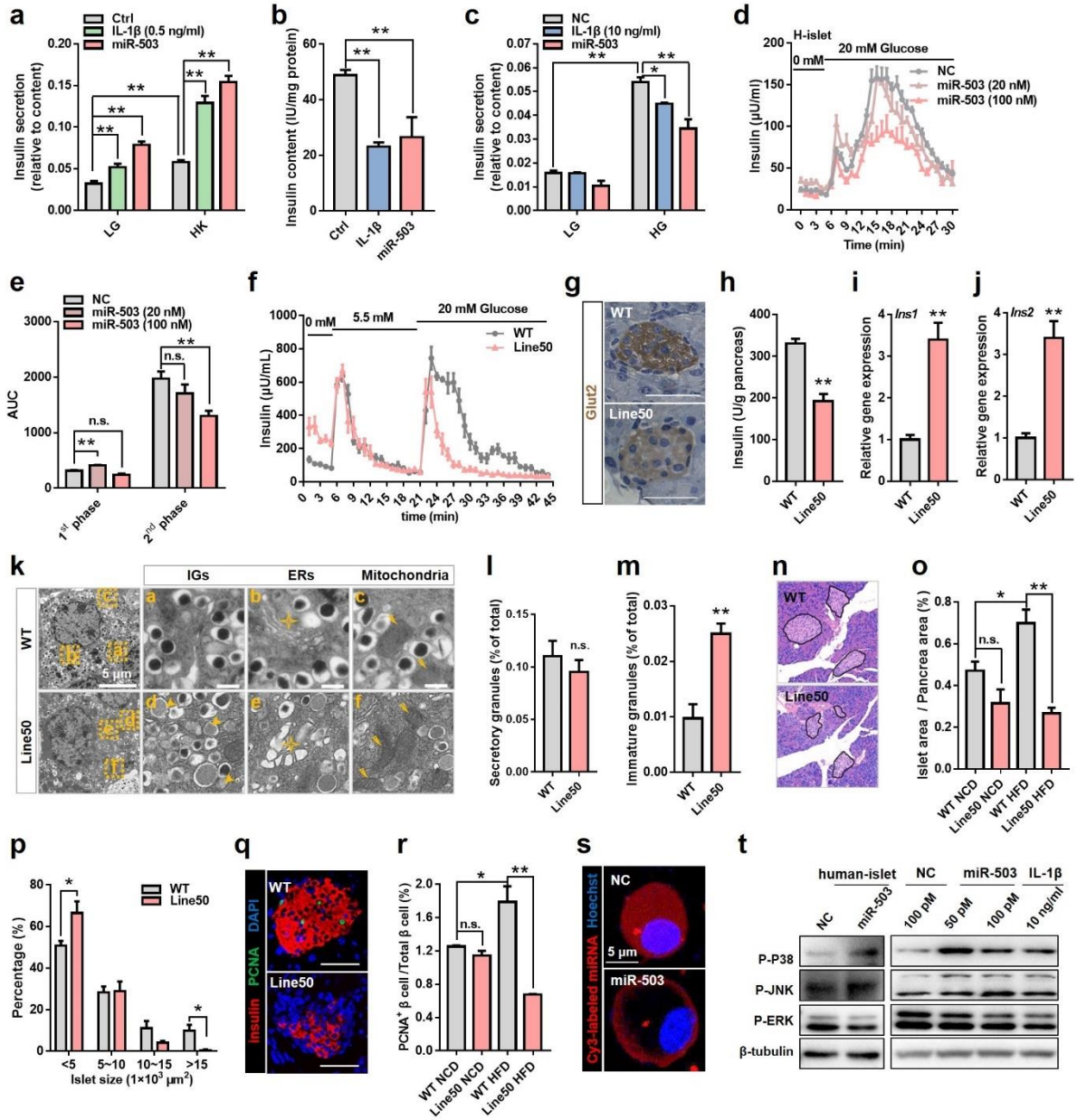

Fig. 5 *miR-503*, Akin to IL-1β Causes β-Cell Defect via Activating MAPK and NF-κB Pathway. **a-e** Cells or primary human islets transfected with NC or *miR-503* mimics for 48h, then insulin secretion and content were assessed by KSIS, GSIS or islets infusion. KSIS (**a**) and content (**b**) of INS-1 cells, GSIS of MIN6 cells (**c**), islet perfusion (**d**) and area under curve (AUC) the first and second phases (**e**) of primary human islets. **f** Islets infusion of 10-week-old WT and Line50 mice islets. **g-j** Representative images

of Glut2 immunohistochemical staining of pancreatic sections (**g**), the white bars refer to 200 μm, insulin content of pancreas standardized by weight (**h**), insulin gene expression in islets (**i, j**) from 10-week-old WT or Line50 mice. **k**-**m** Transmission electron microscopic (TEM) images of the pancreatic islets where orange arrows or stars point to IGs in d, endoplasmic reticulum in b and e, mitochondrial in c and f (**k**), and statistical results of secretory insulin granule (**l**) and ISG (**m**), islets were isolated from 10-week-old Line50 mice and their littermates. **n** Pancreas section from 10-week-old randomly fed mice stained by hematoxylin and eosin (H & E stain). **o** Islet mass represented by area amount percentage of pancreas, and statistical analysis results of islet mass from both NCD and 2-month HFD fed WT or Line50 mice. **p**-**r** Reasons for islet mass decrease, 10-week-old NCD mice islet size distribution (**p**) and PCNA staining of pancreas section represent for evaluation of replication rate (**q**). **s** Primary β cells from 8-week-old male C57BL/6J mice were transfected with Cy3 labeled duplex NC and *miR-503* mimics before which adenovirus were added to media for 1hr. **t** Immunoblot analysis of phospho-p38, phospho-JNK and phosphor-ERK in primary human islets or MIN6 cells transfected with NC or *miR-503* mimics for 48 h. Error bars represent the SEM, N.S. means not significant, *p < 0.05, **p < 0.01, t test, n ≥ 3 per group, TEM and WB were repeated three times.

Beta-cell-derived *miR-503* targets *Insr* to inhibit insulin action in liver and adipose tissues. Careful observation of TEM images from *miR-503*TG islets revealed a considerable number of nanovesicles in mature insulin granules (Fig. 6a, 6b). Judging by their structure and size, these nanovesicles were likely exosomes, which might transport *miR-503* to the extracellular space. We investigated whether insulin granules might be involved in exosomal transportation by dispersing *miR-503*TG islets into single cells, which we then infected with EGFP-NPY adenovirus as a tracer for the insulin granules. The addition of PKH26-labled exosomes to the culture medium resulted in a clear colocalization of the insulin granules and exosomes (Fig. 6c). We further confirmed that the exosomes were residing within the insulin granules by live-cell fluorescence tracing of exosome membrane CD63 with insulin and by immunochemical electron microscopy observation of CD63 within the insulin granules (Fig. 6d; Supplementary Fig. 7a). We confirmed the structure and concentration of β-cell exosomes by TEM and nanoparticle tracking analysis (NTA). The TEM images showed round exosomes with a diameter of about 50 nm (Supplementary Fig. 7b), while the NTA confirmed that exosomes were mostly about 45 nm in size and concentrated in the *miR-503*TG islets (Supplementary Fig. 7c, 7d). After adjustment for protein levels, the released exosomes were determined to package more *miR-503* in *miR-503*TG islets than in WT islets (Supplementary Fig. 7e). Therefore, *miR-503* appears to cause a hijacking of insulin granules to form exosomes, which are then transported for release as granule cargos.

The systematic distribution of β-cell–derived *miR-503* exosomes (*miR-503*-Exos) was determined by analyzing the quantities of *miR-503* in serum, liver, adipose tissue, and skeletal muscle. The *miR-503*TG mice showed significantly elevated *miR-503* levels in serum, liver, and adipose tissue (Fig. 6e - 6g; Supplementary Fig. 7f). Aged Line50 mice (20-week-old) showed comparable serum concentrations of

miR-503 to those found in HFD-fed mice (Fig. 6h). Elevation of circulatory *miR-503* resulted in enrichment of *miR-503* in liver and adipose tissues but not in muscle (Fig. 6i). A similar distribution of *miR-503* was observed in HFD fed mice (Supplementary Fig. 7g). Therefore, we concluded that *miR-503* released from insulin granules can be concentrated in the liver and adipose tissue, where *miR-503* initiates insulin resistance in *miR-503*TG mice, as well as in HFD-fed mice.

The direct effects of *miR-503* were examined by performing an unbiased proteomic analysis in *miR-503* transfected MIN6 cells. Ingenuity pathway analysis (IPA) showed that *miR-503* regulated canonical pathways, including those that enhanced amyloid processing and G1/S checkpoint regulation, as well as inhibiting mTOR signaling and NRF2-mediated oxidative stress responses (Supplementary Fig. 7h). These findings suggested that β cells were in a hypersecreting, proliferative senescent and anti-oxidative failure state, in agreement with the observations in *miR-503*TG islets. The target gene of *miR-503* was identified by cross-analysis of IPA designated upstream regulators with predicted *miR-503* target genes using Targetscan and MiRanda software (Supplementary Fig. 7i). *Rictor*, *Insr*, *Igf1r*, and *Mknk1* were predicted to have seed sequences of *miR-503* (Supplementary Fig. 7j), but *Mknk1* was ruled out as it is a downstream substrate of p38 MAPK and p44/p42 MAPK, both of which were regulated by *miR-503*. We confirmed the inhibitory effect of *miR-503* on *Insr* and *Igf1r* via luciferase activities derived from WT and MUT sequences (Fig. 6j). The protein level of IGF1R was significantly reduced in both INS-1 and MIN6 cells, whereas the INSR level was barely changed in β-cell lines and was even increased in human islets and *miR-503*TG islets (Supplementary Fig. 7k).

These findings suggested that the insulin hypersecretion induced by *miR-503* might restrain INSR processing to degradation. We confirmed this possibility in non-insulin secreting cells, since *miR-503* tended to gather in liver and adipose tissue in vivo. We verified a regulatory role for *miR-503* in primary hepatocytes and mature adipocytes by treating them with supernatant and exosomes from Line50 islets as well as by transfection with double-stranded *miR-503* mimics (Fig. 6k - 6n). Hepatic INSR levels were suppressed by *miR-503* in all cases (Fig. 6m); however, adipose INSR levels were more significantly reduced after administration of insulin (Fig. 6n). Importantly, *miR-503*TG mice showed analogous regulatory effects of *miR-503* on INSR in adipose tissue and liver, as well as no changes in muscle (Fig. 6o). The amount of IGF1R was also decreased in adipose tissue (Fig. 6o). The level of AP-1 suggested that *miR-503* caused a lipogenesis defect in Line58 mice (Fig. 6o), in line with the gene expression levels (Supplementary Fig. 3a). Taken together, these results from in vitro and in vivo

investigations clearly showed that β-cell-derived *miR-503*-exosomes circulate to liver and adipose tissues, where *miR-503* then targets INSR and IGF1R to dampen insulin action.

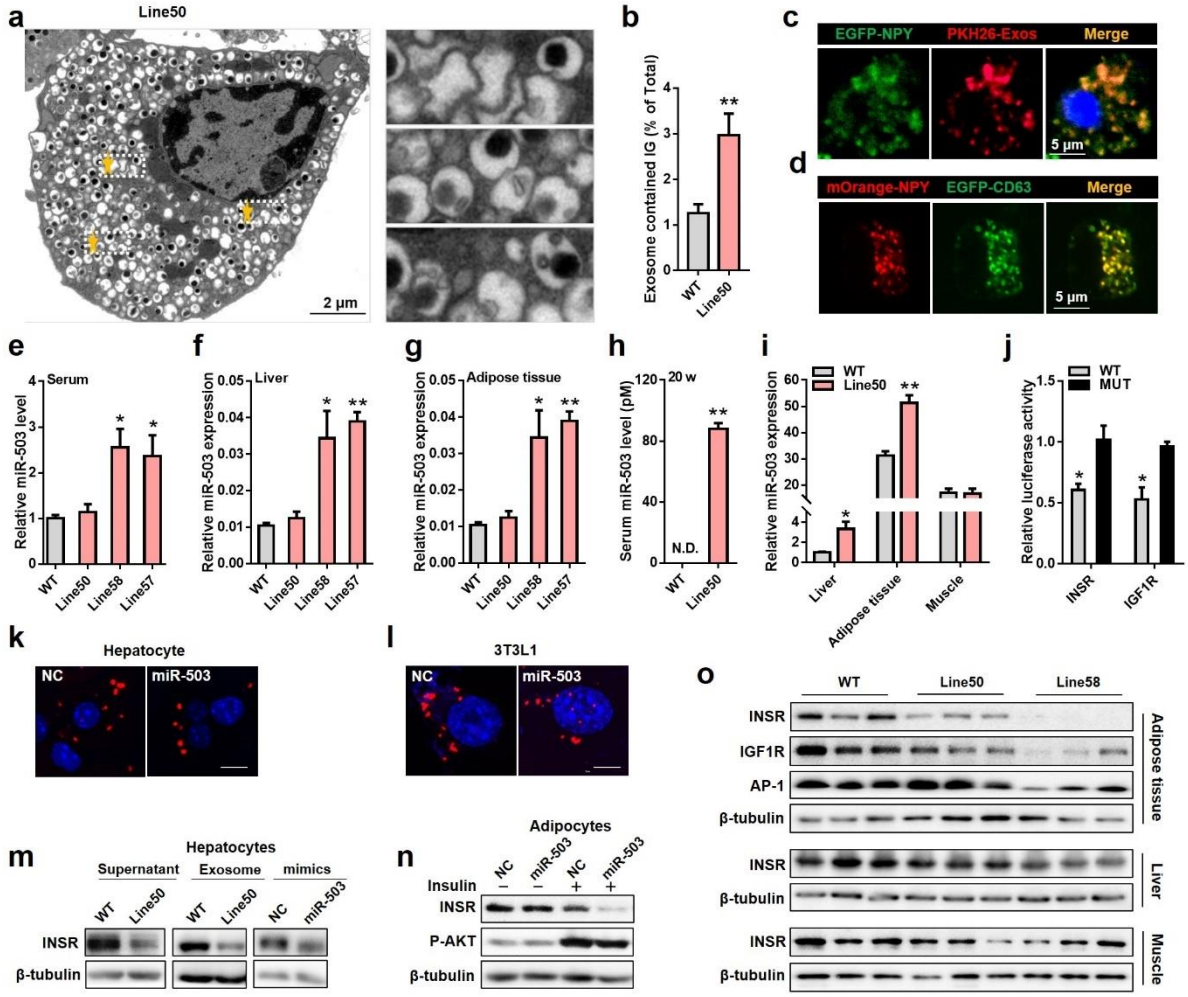

Fig. 6 Beta-Cell Derived *miR-503* Targets Insr to Inhibit Insulin Action in Liver and Adipose Tissue. (**a, b**) TEM photograph (**a**) of β cell from 10-week-old Line50 mice where orange arrows indicate exosome contained IGs and the statistical result (**b**). (**c, d**) Representative images for insulin granule and exosome co-localization, primary β cells from 8-week-old C57BL/6J mice islets transfected with EGFP-NPY adenovirus for 12 h, and PKH26 stained exosomes which extracted from 16-week-old Line50 mice islets were added into media for 8 h (**c**), MIN6 cells co-transfected with mOrange-NPY adenovirus and EGFP-CD63 plasmid for 12 h (**d**). **e-g** *MiR-503* expression in serum (**e**), liver (**f**) and white adipose tissue (**g**) from 8-week-old βTG mice and their littermates. **h, i** *MiR-503* content in serum (**h**) or *miR-503* expression in tissues (**i**) from 16-week-old WT or Line50 mice. **j** Luciferase reporter assay was carried out 24h after 293T cells co-transfected with wt or mut reporter plasmids, PRL-SV40 plasmid and NC, or *miR-503*. **k, l** Images of primary hepatocyte (**k**) or mature adipocyte differentiated from 3T3L1 cells (**l**) transfected for cy3 labeled NC or *miR-503* mimics, the white bar refers to 50 μm. **m** Immunoblot analysis of INSR expression in primary hepatocytes treated with islets supernatant and exosomes extracted from 16-week-old WT or Line50 mice islets, or NC and *miR-503* mimics for 48 h. **n** Immunoblot analysis of INSR and p-AKT expression in mature adipocyte transfected with NC or miR-503 mimics for 48h, before the sample collection 100 nmol/l insulin or physiological saline was added in media for 10 min. **o** Immunoblot analysis of INSR and IGF1R expression in adipose tissue, liver, and skeletal muscle from 8-week-old WT, Line50 and Line58 mice. Error bars represent the SEM, *p < 0.05, **p < 0.01, t test, n ≥ 3 per group, immunofluorescence and WB were repeated three times.

Deletion of the *miR-503* cluster ameliorates HFD-induced insulin resistance in mice. The possibility that ablation of *miR-503* could improve the metabolic disruptions caused by HFD feeding was investigated by global deletion of the *miR-503* cluster (KO mice) (Supplementary Fig. 8a). Deletion of this cluster was confirmed by investigation of genomic DNA and gene expression in metabolic organs (Supplementary Fig. 8b, 8c). The KO mice were healthy and fertile, with no obvious metabolic abnormities. Subjecting the KO mice to HFD feeding for 4 months did not result in any noticeable changes in body weight compared to that of WT mice (Fig. 7a). The levels of fasting blood glucose were also similar between KO and WT mice; however, the levels of refed blood glucose were significantly lower in KO than in WT mice (Fig. 7b). Postprandial insulin levels of serum were also lower in KO mice, with no alterations in fasting settings (Fig. 7c), suggesting that the KO mice were in an insulin-sensitive state. Indeed, insulin tolerance tests (ITTs) clearly showed that KO mice had quick and efficient responses to insulin (Fig. 7d, 7e). Injected insulin lowered blood glucose levels in both KO and WT mice, but the KO mice had a greater response to insulin than WT mice starting at 30 min and thereafter (Fig. 7d, 7e). However, no differences were noted in intraperitoneal glucose tolerance tests (IPGTTs) in the two mouse groups (Supplementary Fig. 8d).

The contribution of *miR-503* target genes to the improvement in ITT results was examined by determining insulin receptor levels in insulin-responsive tissues, including adipose tissue, liver and skeletal muscle. The amounts of INSR protein were comparable between KO and WT mice in all three tissues under the NCD-fed condition (Fig. 7f, 7g), but HFD feeding significantly reduced INSR protein in adipose tissue but not in liver and muscle. Deletion of the miR-503 cluster prevented the reduction in INSR in adipose tissue by HFD feeding (Fig. 7f, 7g). Insulin signal transduction determined by phospho-AKT(S473) expression was significantly improved in KO mice in both adipose tissue and liver (Fig. 7h, 7i). Pancreatic islet mass, β-cell mass, and β-cell function were not affected by miR-503 cluster deletion (Supplementary Fig. 8e - 8i); therefore, the improvements in ITT results were likely attributable to the lack of miR-503 in the serum of KO mice, whereas the serum level was significantly higher in HFD-fed mice than in NCD-fed mice (Fig. 7j). These results supported a role for the miR-503 cluster in the development of insulin resistance, at least in the liver and adipose tissue, during metabolic stress.

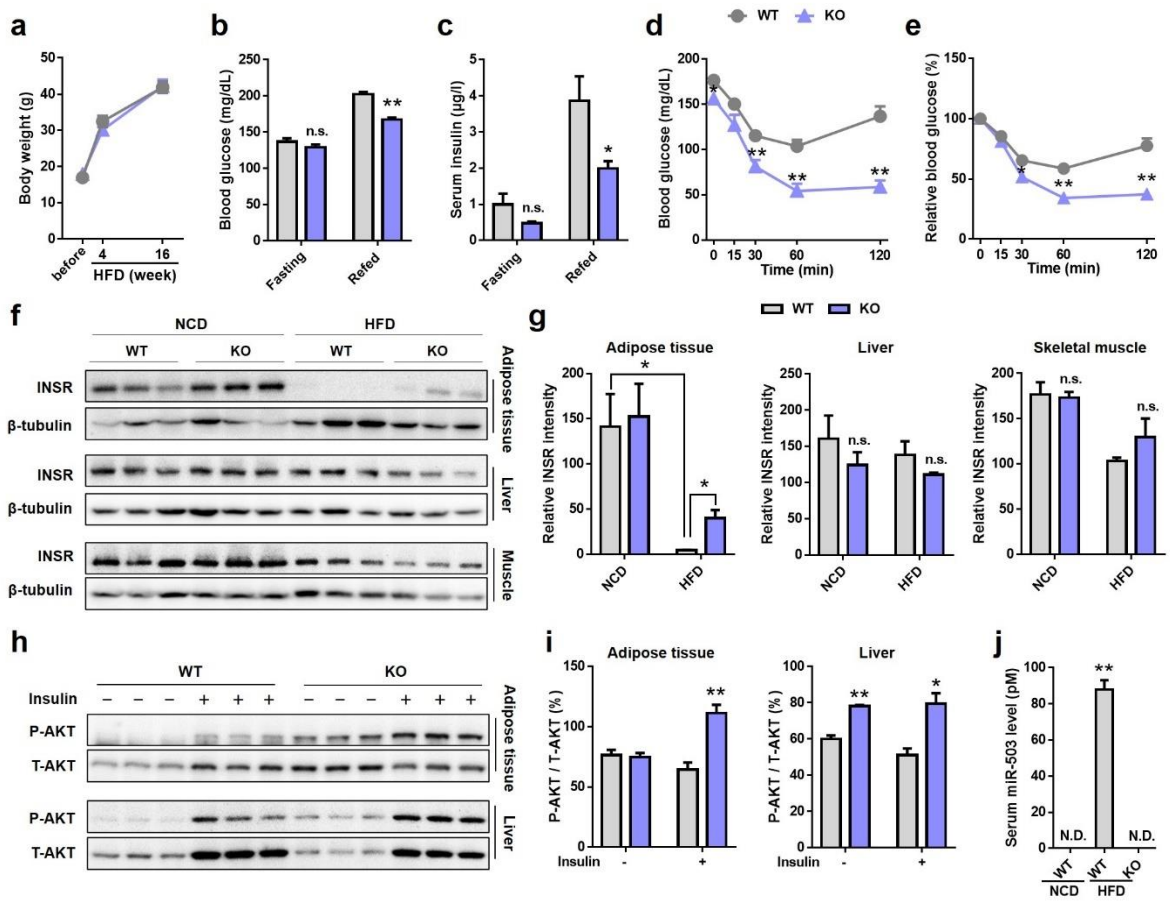

Fig. 7 Deletion of *miR-503* Cluster Ameliorates HFD Induced Insulin Resistance in Mice. **a** Body weight of HFD fed WT or KO mice in accompany with age. **b**-**e** 16hrs fasted and 2hrs after meal blood glucose test (**b**) and serum insulin level (**c**), IPITT (**d**) and standardized IPITT (**e**) of 4-month HFD fed WT and KO mice. **f**, **g** Immuno-blot analysis of INSR expression (**f**) in WAT, liver and skeletal muscle and their gray analysis (**g**). **h, i** 4-month HFD WT and KO mice liver, adipose tissue and skeletal muscle phosphor-AKT and AKT protein expression with or without insulin injection were performed using western blotting (**h**) and their gray analysis (**i**). **j** *MiR-503* contents in mice serum. Error bars represent the SEM, N.D. refers to not detected, *p < 0.05, **p < 0.01, t test, n ≥ 3 per group.

Discussion

The results presented here reveal that β-cell–derived exosomal *miR-503* promotes insulin insensitivity and β-cell aging in the context of chronic inflammation, thereby accelerating β-cell decompensation and diabetes onset. Autocrine exosomal *miR-503* is packed into insulin secretory granules and stimulates P38 MAPK and JNK MAPK but inhibits ERK MAPK to drive β cells from compensatory insulin secretion to decompensatory GSIS defects and growth inhibition and gradually enabling β-cell senescence. The senescent β cells release more exosomal *miR-503*, which then spills into the bloodstream to induce distal effects. The telecrine exosomal *miR-503* that is circulated to insulin-responsive tissues targets *Insr/Igf1r* to dampen insulin signals, particularly in liver and adipose tissues (Fig. 8). Our findings demonstrate that pancreatic β cells could form a metabolic center by secreting insulin, if metabolic

stress and/or aging can control insulin resistance and diabetes progression by releasing exosomal *miR-503*.

The elevation in circulating *miR-503* in patients with T2D, as well as in HFD-fed and aged mice, as shown here, might stem from β cells that experience a prolonged IL-1β/IL-1R1 activation, since β cells have the highest numbers of IL-1 receptors on their cell surfaces. The promotor region of *miR-503* is hypomethylated in patients with T2D, and activation by IL-1β assures that the β cells act as generators of *miR-503* under metaflammation and inflammaging conditions, probably via the IKK/NF-κB pathway. A variety of stimuli, such as nutrients, cell debris, and misplaced molecules, sustain tissue inflammation in distinct organs, including adipose tissue, liver, and pancreas.

Extensive research now indicates that local inflammation in adipose tissue can have systematic effects due to secretion of proinflammatory factors and miRNAs derived from extracellular vesicles. The possibility that metaflammation-adapted and inflammaging-adapted β cells cause systematical insulin resistance remains to be established. The β cells renew slowly by self-replication, so they are sensitive to the metabolic burdens imposed by obesity and aging. Persistent stresses from unfolded protein responses (UPRs) and reactive oxygen species (ROS)-mediated modifications in β cells creates a proinflammatory islet microenvironment and resulting islet inflammation (insulitis).

Insulitis usually precedes the onset of frank diabetes and is a common feature of type 1, type 2, and aging-related diabetes, with IL-1β as a common executor. Physiological levels of IL-1β stimulate insulin to promote postprandial glucose disposal, whereas supraphysiologic IL-1β can inhibit the function and reduce the mass of β-cells by triggering signaling cascades from membranous IL-1 receptors to downstream MAPK and IKK effectors to activate AP-1 and NF-κB. Insulitis also generates an endogenous anti-IL-1 molecule, interleukin 1 receptor antagonist (IL-1Ra), which blocks the prolonged IL-1β effects[23]. Some reports have shown that plasma levels of IL-1Ra significantly increase in obese humans and rodents and positively correlate with insulin resistance and diabetes onset[24]. The levels of IL-1Ra are decreased in islets from T2D patients and fail to protect β-cell compensatory expansion due to the diminished production of IL-1Ra by the β cells themselves[25].

The seemingly incompatible levels of IL-1Ra in circulation and in β cells strongly suggest that other molecules may also contribute to IL-1β-induced β-cell decompensation and systematic insulin resistance. In our opinion, *miR-503* may serve this function. A gene-regulating effect of *miR-503* in insulin-responsive tissues and a ligand-like effect of *miR-503* in β cells could explain the poor

effectiveness of anti-IL-1 approaches in HbA1c control in patients with T2D, despite a great improvement in β-cell function. Other molecules, such as *miR-26*, *miR-29*, and *miR-375*, may also contribute to insulin resistance and β-cell dysfunction in response to chronic inflammation[26–28].

The *miR-503/322* cluster, which is highly expressed in the developing pancreas in E16.5 mice, shows gradually decreasing expression postnatally and maintains this low expression level in mature pancreatic islets. The loss of miRNA processing by Dicer deletion uniquely impairs the development of endocrine lineage[29]; therefore, embryonic expression of *miR-503/322* may be particularly important in β cells. Indeed, Francis et al. have reported that *miR-503* is colocalized with the β-cell determinant Pdx1 in the pancreas[17]. Our findings and those of other groups support the importance of *miR-503* in β-cell genesis and that its decrease may ensure rapid β-cell expansion and replication at postnatal 2 - 4 weeks.

The re-expression of *miR-503* in mature β cells from rodents to humans in conditions of metaflammation and inflammaging may cause a compensatory decrease in β-cell expansion. Indeed, our data from mice with β-cell–specific overexpression of *miR-503* show that *miR-503* dramatically inhibits postnatal (Cluster TG, Line58, and Line57), as well as metabolic stress-imposed (Line50), β-cell replication by IL-1β-like activations of the MAPK and NF-κB pathways. The colocalization of *miR-503* and IL-1R supports the conclusion that *miR-503* mimics IL-1β function by acting as a ligand of IL-1R or other membranous receptors, but not as a gene regulator, in β cells. More importantly, collective evidence from single-cell RNA sequencing, as well as the expression levels of classic senescence genes and insulin genes, supports the promotion of β cells into a prematurely senescent state by *miR-503* to maintain its compartmentation in exosomes and release from insulin granules.

We have no direct evidence that shows how *miR-503* triggers β-cell senescence, but infiltrating $Ccr6^+$/$Ccr7^+$ immune cells might be involved, as Ccr7 intimately interacts with proteins that increase in senescent β cells (Supplementary Fig. 9). Further investigations, like blocking $Ccr6^+$/$Ccr7^+$ immune-cell infiltration, might add support for our proposed mechanism to explain how *miR-503* drives β-cell senescence. The observation that senolysis (elimination of senescent cells) is a preventive and alleviating strategy for both T1D and T2D strengthens our proposal that molecules like *miR-503*, upon release from aging β cells, might trigger diabetes onset as a result of both insulin resistance and β-cell dysfunction[30,31].

Our finding that *miR-503* exosomes are located in insulin granules was serendipitous but extremely thrilling. Exosomes are nano-vesicles 30 –150 nm in size and are produced by multiple cell types. They

which originate from the fusion of late endosomes/multivesicular bodies (MVBs) with the cell plasma membrane[32]. Upon their release into the extracellular environment, exosomes can fuse with live cells and transfer their cargos of proteins, lipids, and RNAs into the acceptor cells[33]. In this case, these are cells that are closely associated with obesity and diabetes. Endocrine β cells release exosomes under normal circumstances, but they change their exosomal cargos in response to different stimuli[34]. By contrast, islet exosomes promote insulin action and glucose tolerance in local and distal organs by the transfer their miRNA cargos (e.g., *miR-26*)[27]. These findings emphasize that β cells release exosomes both in vivo and in vitro and that deregulation of exosomes contributes to diabetes progression. However, the precise location of these exosomes within the β cells remains elusive.

Recently, the insulin granule, which has a diameter of 300 - 350 nm, has been proposed to serve as a signaling hub rather than simply functioning as an insulin container[35]. Co-secreted compounds, including amylin and γ-amino butyric acid (GABA), also have important metabolic regulatory functions. The presence of exosomes in insulin granules has never been reported before. Our TEM, immunogold staining, and live-cell imaging results confirm that exosomes, with a diameter of 45 nm, reside within the β-cells in this unique organelle, the insulin granule. Primary β cells contain approximately 10,000 insulin granules, corresponding to 10 – 20% of the total cell volume, thereby providing a large exosome reservoir. The insulin granule has a half-life of three days, which ensures an opportunity for exosome formation.

The process by which the insulin granule encapsulates exosomes might be controlled by specific miRNAs based on their sequences, as *miR-503* overexpression significantly increases the number of exosome-containing insulin granules. Alternatively, *miR-503* inhibition of ERK MAPK signaling may facilitate exosomal *miR-503* formation in the insulin granules, consistent with the literature showing that inhibition of KRAS-MEK signaling boosts Ago2-associated miRNAs sorting into exosomes[36]. The mechanism by which miRNA and miRNA-associated proteins are sorted into insulin granular exosomes requires further study, especially since our finding does not exclude multivesicular bodies (MVBs) as an origin of the exosomes in β cells. Nonetheless, our data indicate that a diabetes-associated exosomal *miR-503* resides within the β-cell insulin granule and this finding enriches the current knowledge of insulin granule contents.

Exosomal *miR-503* released by mouse islet β cells directly triggers insulin resistance in liver and adipose tissues, in part by downregulating *Insr* and *Igf1r* expression. The discovery of *Insr/Igf1r* is based

on unbiased proteomic data by comparing differential expression of proteins between *miR-503*-expressing and control miRNA–overexpressing MIN6 cells. The regulatory role between *miR-503* and *Insr/Igf1r* was confirmed by 3'UTR seed-sequence based luciferase activity and protein abundance in MIN6 cells and INS-1 cells, two widely used β cell lines. However, the protein levels of INSR/IGF1R were enhanced, rather than reduced, in primary islets from *miR-503*TG mice and from *miR-503* transfected human islets. The discrepancy in the results between β cell lines and primary islets may reflect the insulin secretory abilities that enable insulin receptors boosted by autocrine insulin to compensate for the reduction of these receptors in *miR-503*-overexpressing β cells[37]. Alternatively, the hypersecretion ability of primary β cells could promote exosomal *miR-503* release, thereby minimizing the cellular *miR-503* levels and reducing its gene regulatory effect in human and mouse islets.

The fasting serum insulin level of *miR-503*TG mice is barely altered, regardless of how many β cells remain, suggesting that insulin receptors in peripheral tissues are unlikely to be affected by circulatory insulin levels. Therefore, the significantly decreased levels of insulin and IGF1 receptors in insulin-responsive tissues solely originate from the elevation of *miR-503* levels in the *miR-503*TG mice as well as in HFD-induced mice, at least in the adipose tissues. Mice with tissue-specific deletion of insulin and IGF1 receptors in liver, muscle, adipose tissue, and β cells display insulin resistance, β-cell decompensation, glucose intolerance, diabetes, and early death, largely akin to the phenotypes of our *miR-503*TG mice[38–40]. The expression of *miR-503* also determined the extent of preadipocyte maturation in company with insulin, as indicated in both the *miR-503*TG mice and global *miR-503* cluster KO mice, with the most pronounced abnormities noted in adipose tissue. This defect likely arises from the loss of IGF1 receptors in the adipose tissue of *miR-503*TG mice, considering the relatively high expression level of IGF1R compared to INSR in human preadipocytes. Coincidently, David et al. have reported that KO mice show a higher body weight due to increased white fat content at a later age, suggesting an essential role of the miR-503 cluster in mature adipocytes.

Whether the combined loss of insulin and IGF1 receptors is the cause of HFD-induced adipose expansion failure remains to be established. Our in vivo results, in conjunction with the data on in vitro exosome delivery of *miR-503* in primary hepatocytes and adipocytes, support a suppression of insulin and IGF1 receptors by *miR-503* that disrupts insulin signaling and triggers insulin resistance. We did not pursue other *miR-503* targets for their contributions to the diabetes phenotype of *miR-503*TG mice since the main defects are largely covered by INSR/IGF1R inhibitions. Some studies have implicated

miR-503 in angiogenesis, mammary epithelial involution after pregnancy, and myotube formation via diverse target-dependent effects, but a role for exosomal *miR-503* release from β-cells in insulin resistance in distal organs has not been previously appreciated.

Premature death is a common phenotype in the Line57 and cluster TG mice. Dissection of weak mice showed multiple organ failure (MOF), including the liver and gut. The abdominal distension and the intestinal color indicated that the Line57 and cluster TG mice might die from infection. The association between diabetes and infection is well known clinically, and aging patients with T2D are more vulnerable to frequent and serious infections[41]. Diabetes increases the infection risk mainly because of chronically hyperglycemic environments. Causal pathways include impaired immune responses as well as other diabetes associated abnormalities, such as neuropathy and vascular insufficiency. Our analysis of the glucose-intolerant Line50 mice revealed a decrease in principle cytokine genes, including *IFNα*, *IL6*, and *IL10* in the *miR-503*TG islets, indicating an immunosuppressive role for *miR-503* independent of hyperglycemia. Single-cell RNA sequencing affirmed the reduction in endothelial cell numbers in *miR-503*TG islets, suggesting that the increased infection risk is also associated with defective angiogenesis due to *miR-503*, consistent with an earlier finding that *miR-503* impairs post-ischemic angiogenesis in limb muscles. Therefore, our findings demonstrate that *miR-503* can increase the infection risk by direct immune suppression and anti-angiogenesis functions, rather than by an indirect action due to hyperglycemia. Therefore, the contribution of *miR-503* to host-pathogen interaction and infectious diseases is an additional promising area of research. Prospects for the development of anti-*miR-503* therapies to reduce diabetes and infection risk are also good, based on our study.

In summary, our study reveals a metaflammation-related and inflammaging-related involvement of *miR-503* in determining type 2 diabetes that leads to insulin resistance and β-cell dysfunction. This *miR-503* activity also increases the infection risk with age in severe diabetes settings. Thus, therapeutic strategies aimed at blocking *miR-503* generation in β cells may prove to be a promising approach for preventing insulin resistance, β-cell decompensation, and diabetes onset, as well as diabetes-associated infection.

Methods

Cell culture. Rat insulinoma cell line INS-1 cells (ATCC CM-1421) were cultured in RPMI 1640 (Invitrogen, Grand Island, NY) media containing 10% FBS (Gibco, 12483020). Mouse pancreatic β cell line MIN6 cells (Miyazaki, 1990) were cultured in DMEM

media, containing 15% FBS. Both media were supplemented with 100 mg/mL streptomycin, 100 units/mL penicillin, 10mM HEPES and 50 μM β-mercaptoethanol (Sigma-Aldrich, M6250). 293T cells were cultured in DMEM media, containing 10% FBS, 100 mg/mL streptomycin, 100 units/mL penicillin. Thapsigargin (Sigma, T9033) and 5-Azacytidine (APExBIO, A1907) were added in the medium for 48 h to test miR-503 expression in accompany with DNA modification.

The embryonic fibroblast mouse cell line, 3T3-L1 (American Type Culture Collection), was cultured and differentiated as described previously[42] and in ESM Methods. The medium was replaced every 2 - 3 days. Passages 5 - 6 were used for all experiments. All cells were cultured at 37°C in a humidified atmosphere containing 95% air and 5% CO_2.

Animal care. β-cell specific *miR-503-322-351* transgenic mice (RIP2-*miR-503-322-351* TG, Cluster TG) and *miR-503* transgenic mice (RIP2-*miR-503* TG, *miR-503* TG) were generated by GemPharmatech Co，Ltd (Nanjing, China) by using rat insulin 2 gene promoter (RIP2). Chimeric mice were inbreeded with C57BL/6J mice at least twice to generate genetic stable pups for the study use. However, the offspring (F1) of Cluster TG chimeric mice couldn't survive to reach sexual maturity then the F1 mice were used to analyze. Three founder lines with different copies were obtained from the second generation of *miR-503* TG mice, Line50 (5.2), Line58 (13.3), and Line57 (22.9). Global deletion of *miR-503-322-351* mice (KO), were generated by GemPharmatech Co，Ltd (Nanjing, China) through CRISPR/Cas9 technology.

Male C57BL6/J mice, non-obese diabetic (NOD) mice, lepr (db/db) mice and Goto-Kakizaki rats were purchased from GemPharmatech Co，Ltd. Mice including Line50, KO and their littermates were feed with high fat diet (HFD, 60% of kcal from fat, 20% kcal from carbohydrate and 20% of kcal from protein, Research Diets) since 4-weeks-old and continued to 12 or 20 weeks of age respectively. All mice were housed at a 12 h light/dark cycle at 23 - 25°C and animal studies were approved by the Research Animal Care Committee of Nanjing Medical University. βTG mice and their littermate were provided with either a standard chow or high fat diet (HFD, 60% of kcal from fat, 20% kcal from carbohydrate and 20% of kcal from protein, Research Diets). HFD was given to mice at 7-week-old and continued to 20-week-old.

Primary islet isolation and culture. Human islets were provided from Tianjin First Central Hospital. The use of human islets was approved by the research ethics committee of Nanjing Medical University. The use of human islets was approved by the research ethics committee of Tianjin First Central Hospital. Murine islets were isolated and cultured as described previously[43]. Isolated islets were cultured in RPMI medium (glucose: 5.5 mmol/L) containing 10% FBS, 100 units/mL penicillin, and 100 mg/mL streptomycin at 37°C in a humidified 5% CO_2 atmosphere.

Primary hepatocytes isolation and culture. The hepatocytes were isolated from male 8-week-old C57/B6J mice fasted for 6 h.

The viability of freshly isolated cells was examined using trypan blue (Sigma, 93595) ensuring more than 90% viability. After the hepatocytes were attached to dishes in DMEM-low glucose (5.5 mM) plus 10% (vol/vol) FBS for 4 h, the medium was changed to DMEM-low glucose containing 0.1% bovine serum albumin (BSA) (wt/vol) (Sigma, V900933) for further studies on the same day.

Metabolic characters and ELISA. Blood samples were collected from tail vein and blood glucose level were measured using a Glucometer Elite monitor (Abbott, FreeStyle Optium Neo H). Mice were fasted for 14-16 h, then fasting-blood-glucose (FBG) or GTTs were measured, dosage of D-glucose was 1 g/kg and injected through intraperitoneal (I.P.). After 14-16h fasting mice were fed and 2 h late the refed blood glucose was measured. ITTs were performed by I.P. injection of 1.0 units/kg insulin after 4 h of fasting. Mice whole bloods were centrifuged at 3000g for 20 min to collect serum. Serum insulin, C-peptide and Glucagon were measured separately by Insulin Elisa kit (Mercodia, 10-1247-0), c-peptide Elisa kit (ALPCO Diagnostics, 80-CPTMS-E01), and Glucogan Elisa kit (Elascience, E-EL-M0555c).

Hyperinsulinemic-euglycemic clamps. Preparation of the mice was same with hyperglycemia clamp assay. Mice were equilibrated from t= -90 to 0 min after 4-6 hours fasting. [3-^{3}H] glucose (3 μCi, Moravek, MT-914) was administered at t = −90 min, followed by a constant infusion of 0.05 μCi/min. After 90 min as a basal period (t = −90 to 0 min), blood samples were collected from tail vein for determination of plasma glucose concentration and basal glucose specific activity. Then the continuous of human insulin (Wanbang Biopharmaceuticals) infusion was started (t = 0 min) at a rate of 4 mU/kg/min to keep hyperinsulinemic condition with submaximal suppression of HGP to assess insulin sensitivity. At 0 min, the continuous infusion rate of [3-^{3}H]-D-glucose tracer was increased to 0.15 μCi/min for minimization of the changes of glucose specific activity. At t = 75 min, 10 μCi 2-[^{14}C] D-glucose (Moravek, MC-355) was administered into each mouse to measure glucose uptake. Blood samples were collected at 10 min intervals from tail vein, blood glucose concentrations were measured by a glucose meter. During the 120 min clamp, variant glucose was simultaneously infused to keep the blood glucose concentration stable (~130 mg/dL). The glucose infusion rate (GIR) was recorded to assess insulin sensitivity. At the end of clamp, additional blood samples were collected to determine the plasma glucose concentration and glucose specific activity. Liver, muscle, and adipose tissues were collected for the determination of radioactivity. Serum and tissue radioactivity were measured and calculated as previously described[44].

Insulin sensitivity evaluation of liver, muscle and adipose tissue. Mice were i.p. injected with 2 units/kg insulin or saline after 5 h of fasting. 10 minutes after injection, mice were sacrificed then liver, muscle adipose tissues were collected for western blotting and qPCR.

Islet perfusion. After equilibrating overnight, 120 islets per group were incubated 1 hour at 37 °C in Krebs-Ringer buffer (KRB)

solution with 0 mM glucose. Then islets were collected in a syringe filter (Millipore, Millex-GP) for further perfusion. 37 °C KRB solution with 0 mM glucose were perfused at 125 μL/min for 15 minutes to equilibrate, then the perfusate were collected per minute for another 6 minutes. After that, 37 °C KRB solution with 20 mM glucose were perfused for 25 minutes and the perfusate were collected as previous. 7 - 12 min was determined as the first phase insulin secretion while 12 - 30 min was defined as the second phase of insulin release. The insulin levels of the perfusate were measured by radioimmunoassay (RIA) as previously described[45].

Islet-derived exosomes isolation and NTA. Isolated islets were cultured in a serum-exosomes-free culture media (11.1 mM glucose) for one week, the media was replaced and collected every 24 h. Media were firstly centrifuged at 700g for 5 min to pellets cells, and 10000g for 1 h to discard dead cells and cell debris. For cell treatment use, exosomes were isolated by adding half volume of supernatant exosome isolation reagent (Invitrogen, 4478359) overnight, and then centrifuged at 10000g for 1 h. For NanoSight particle tracking analysis (NTA), exosomes were isolated from the supernatant by ultracentrifugation at 100,000g for 2 h. Exosomes were collected in a minimal volume of RNase free PBS, then applied to a blue laser beam at 405 nm. NTA software analyzed the samples and calculated exosomes particle size and concentration.

Islets single cell dissociation and scRNA sequencing. Firstly, isolated islets were cultured in culture media (5.5 mM glucose) for 4 h. Secondly, islets were picked into 10 ml sterile cuvette and digested with 1 ml 0.08% Trypsin/EDTA for 5 min at 37 °C atmospheres. Thirdly, 2 ml culture media with 10% FBS was added into cuvette to suspend the digestion, disperse islets with micropipette. Finally, cells were centrifuged at 1000 rpm for 5 min, then discard supernatant and suspend cells with serum free media. The viability of freshly isolated cells was examined by cell counter (Ruiyu Biotech, IC1000) to ensure more than 90% viability. 10x Genomics Chromium platform was used to prepare single-cell RNA sequencing library. The resulting libraries were sequenced on an Illumina NovaSeq 6000 System. The data cleaning, normalization and scaling were handled by Novogene company as previously described[46].

The PCA analysis was used to reduce dimension and cell types were clustered through a k-means-based approach implemented in Seurat. Following clustering, all cells were projected onto a two-dimensional map by means of t-SNE. Marker genes of each cell cluster were outputted for GO and KEGG analysis to define the cell types. The pseudo-temporal ordering and gene regulatory network analysis were reported as previously[47].

RNA extraction, quantitative and absolute quantitative real-time PCR. Cell supernatant and serum RNA were extracted by Trizol LS (Invitrogen, 10296010) while total RNA was extracted using Trizol (Invitrogen, 15596026). The reverse transcriptions of pri-miRNA, miRNA and mRNA were performed as previously described[43]. Quantitative real-time PCR was performed using the

THUNDERBIRD probe qPCR Mix (TOYOBO, QPS-101) for primary and mature miRNA, and SYBR Green qPCR Master Mix (Vazyme, Q111-02) for mRNA on Roche Lightcycle480 II Sequence Detection System (Roche Diagnostics). qPCR primers for pri-miRNA and miRNA were purchased from Thermofisher Co., Ltd, other primers sequences are available in Supplementary Table1. For absolute quantitative real-time PCR, *cel-miR-39-3p* was used as standards, the reverse transcription and qPCR reaction system were performed according to the manufacturer's instructions (RiboBio, miRB0000010-3-1, MQPS0000071-1-100, MQPS0002912-1-100, MQPS0001690-1-100).

Plasmid construction and luciferase assay. The wild-type (wt) and mutant (mut) 3' UTR-luciferase constructs of mouse *INSR* and *IGF1R* were generated by annealing and cloning the short sequences into pMIR-REPORT Luciferase miRNA Expression Reporter Vector (Ambion, Foster City, CA) between the SpeI and HindIII sites. Primer sequences are as followings: wt-*INSR* (5'-CTAGTAATTGACCAATAGCTGCTGCTTTCA-3', 5'-AGCTTTGAAAGCAGCAGCTATTGGTCAATT-3'), mut-INSR (5'-CTAGTAATTGTCGATTAGCAGGTCCATTCA-3', 5'-AGCTTTGAATGGACCTGCTAATCGACAATT-3'), wt-IGF1R (5'-CTAGTTACAGGAAAAGAAAAGCTGCTACTG-3', 5'-AGCTTCAGTAGCAGCTTTTCTTTTCCTGTA-3'), mut-IGF1R (5'-CTAGTTATATGCAAAGAAAAGATACGACTG-3', 5'-AGCTTCAGTCGTATCTTTTCTTTGCATATA-3'). The reporter plasmid, pNF-κB luciferase reporter plasmid containing the NF-κB-enhancer consensus sequences [(TGGGGACTTTCCGC)×5] was purchased from Stratagene (La Jolla, CA, USA). Luciferase activities were measured using the Dual-Glo Luciferase Assay System (Promega, Madison, WI) on a TD-20/20 Luminometer (Turner BioSystems, Sunnyvale, CA) according to the manufacturer's protocols.

Transient transfection and adenovirus infection. MiRNA duplex mimics, cy3-labeled single strand miRNA or duplex miRNA mimics, were obtained from GenePharma. For transient transfection, Lipofectamine 2000 reagent (Invitrogen, 11668027) was mixed with miRNA mimics, or overexpression/reporter plasmids as previously described[45].

The enhanced green fluorescent protein (EGFP) or mOrange tagged NPY adenovirus was diluted with a serum-free medium at a concentration of 2.0×10^6 pfu/ml for dissociated islet cells and MIN6. Cells were plated in 3.5-cm Greiner dishes, the culture media was firstly discarded, then the prepared adenovirus-containing culture solution was added to incubated for 2 h in the incubator. At last, it was replaced with fresh complete medium to continue culturing 2-12 h.

Fluorescence labelling of exosomes and confocal live-cell imaging. Exosomes were labelled with PKH26 (Sigma, MINI26) for 1 h and then washed three times with PBS. PKH26-labelled exosomes were resuspended in RPMI-1640 or DMEM media and incubated with dissociated islet cells for 4 h.

For live-cell imaging, MIN6 co-transfected with mOrange-NPY and EGFP-CD63, or dissociated islet cells transfected with EGFP-NPY and stained exosomes were cultured in a heated, gas-perfused chamber at 37°C with 5% CO_2 and visualized with a

laser scanning microscope (Olympus, FV1200).

Cell counting kit-8 assay. Transfected cells (1×10^3 per well) in 100 μl complete medium were seeded in 96-well plates and cultured overnight. After the overnight culture, the cells were treated with CCK-8 solutions (Beyotime, C0037) and incubated at 37°C for 2 h. The absorbance at 450 nm was measured by a microplate reader.

Insulin secretion assay. MIN6 or INS-1 cells were seeded in 48-well plates and transfected with NC or miR-503 mimics for 48 h, the insulin secretion capacity was detected by GSIS or potassium-stimulated insulin secretion (KSIS) assays as previously described[45].

Western blot analysis. Western blotting was performed as previously described[48]. The antibodies used are listed in Supplementary table2. Stripes intensity was measured by Image J (NIH Image, Bethesda, MD).

Mass spectrometry analysis. MIN6 cells were washed with ice-cold PBS, collected, and dissolved in lysis buffer (7 mol/L urea, 1% CHAPS). Protein digestion, tandem mass tag labeling, and mass spectrometry analysis then were conducted at the Analysis Center of Nanjing Medical University as previously described[48].

Immunofluorescence, immunohistochemical, H&E staining and TUNEL assay. Immunofluore-scence for Insulin (Santa Cruz, CA, USA), Glucagon (Phoenix peptide, G-028-02), Polypeptide (Phoenix peptide, H-054-02), Somatostatin (Abcam, Ab30788), PCNA (Abcam, Ab92552) and Ki67 (Service Bio, GB11030) were performed on 4% paraformaldehyde-soaked pancreatic sections. The section was incubated with first antibody (diluted 1:100 in 3% BSA) at 37 °C for 2 h and Alexa Fluor–conjugated secondary antibodies (Invitrogen, diluted 1:500 in the same dilution buffer) at 37°C for 1.5 h. Then, 5 μg/ml Hoechst 33342 were used to stain the nucleus for 15 min and washed with PBS. Finally, we use a confocal laser scanning microscopy system to capture and analysis the coverslips. For immunohistochemical staining, mouse pancreas was isolated and fixed with 4 % paraformaldehyde in PBS, then embedded in paraffin. Paraffin-embedded samples were cut (5 μm) and sections were incubated overnight at 4°C with a rabbit monoclonal antibody against Glut2 (Santa Cruz, sc-518002, 1:100). Detection was performed with a secondary antibody provided in the Mouse/Rabbit ImmunoDetector HRP/DAB Detection System (Gene Tech, GK500705).

The H&E staining of all samples was done by Wuhan Servicebio Technology CO., LTD. The whole sections were scanned with Pannoramic 250 (3D HISTECH) and examined with Pannoramic Case Viewer V2.3.0. Apoptotic cells in primary islets were measured using a TUNEL kit (Vazyme, A111-02) and performed according to the manufacturer's instructions.

Statistical analysis. In vitro experiments were repeated at least three times and in vivo assay were repeated two times, with the number of per condition or mice included in each group in each experiment indicated. Single-cell RNA-seq were analyzed as

described above. Additional data were plotted and analyzed using the GraphPad Prism 8.0 software (GraphPad Software, San Diego, CA). Comparisons were performed using the Student t test between two groups. Results are presented as mean ± SEM. P <0.05 is considered statistically significant.

Reporting summary. Further information on research design is available in the Nature Research Reporting Summary linked to this article.

Data and code availability

The single-cell sequencing data have been deposited to the Gene Expression Omnibus (GEO) database repository with the dataset identifier GSE155798. All other supporting data in this study are available from the Lead Contact on request.

References

1. Taniguchi, C. M., Emanuelli, B. & Kahn, C. R. Critical nodes in signalling pathways : insights into insulin action. **7**, 85–96 (2006).
2. Samuel, V. T. & Shulman, G. I. Mechanisms for insulin resistance: common threads and missing links. *Cell* **148**, 852–871 (2012).
3. Mezza, T. *et al.* β-Cell Fate in Human Insulin Resistance and Type 2 Diabetes: A Perspective on Islet Plasticity. *Diabetes* **68**, 1121–1129 (2019).
4. Eguchi, K. & Nagai, R. Islet inflammation in type 2 diabetes and physiology. *J. Clin. Invest.* **127**, 14–23 (2017).
5. Dror, E. *et al.* Postprandial macrophage-derived IL-1 盞stimulates insulin , and both synergistically promote glucose disposal and inflammation. (2017) doi:10.1038/ni.3659.
6. Sauter, N. S., Schulthess, F. T., Galasso, R., Castellani, L. W. & Maedler, K. The antiinflammatory cytokine interleukin-1 receptor antagonist protects from high-fat diet-induced hyperglycemia. *Endocrinology* **149**, 2208–2218 (2008).
7. Consortium, I. 1 G. Cardiometabolic effects of genetic upregulation of the interleukin 1 receptor antagonist: a Mendelian randomisation analysis. *lancet. Diabetes Endocrinol.* **3**, 243–253 (2015).
8. Christensen, D. P. *et al.* Lysine deacetylase inhibition prevents diabetes by chromatin-independent immunoregulation and β-cell protection. *Proc. Natl. Acad. Sci. U. S. A.* **111**, 1055–1059 (2014).
9. Guay, C. *et al.* Lymphocyte-Derived Exosomal MicroRNAs Promote Pancreatic b Cell Death and May Contribute to Type 1 Article Lymphocyte-Derived Exosomal MicroRNAs Promote Pancreatic b Cell Death and May Contribute to Type 1 Diabetes Development. 348–361 (2019) doi:10.1016/j.cmet.2018.09.011.
10. Rupaimoole, R. & Slack, F. J. cancer and other diseases. *Nat. Publ. Gr.* (2017) doi:10.1038/nrd.2016.246.
11. Krol, J., Loedige, I. & Filipowicz, W. The widespread regulation of microRNA biogenesis, function and decay. *Nat. Rev. Genet.* **11**, 597–610 (2010).
12. Heil, F. *et al.* Species-Specific Recognition of Single-Stranded RNA via Toll-like Receptor 7 and 8. **303**, 1526–1530 (2004).
13. Fabbri, M. *et al.* MicroRNAs bind to Toll-like receptors to induce prometastatic in fl ammatory response. **109**, (2012).
14. Massart, J. *et al.* Altered miR-29 Expression in Type 2 Diabetes In fl uences Glucose and Lipid Metabolism in Skeletal Muscle. **66**, 1807–1818 (2017).
15. Wang, F. *et al.* H19X-encoded miR-424(322)/-503 cluster: emerging roles in cell differentiation, proliferation, plasticity and metabolism. *Cell. Mol. Life Sci.* **76**, 903–920 (2019).

16. Taganov, K. D., Boldin, M. P., Chang, K.-J. & Baltimore, D. NF-kappaB-dependent induction of microRNA miR-146, an inhibitor targeted to signaling proteins of innate immune responses. *Proc. Natl. Acad. Sci. U. S. A.* **103**, 12481–12486 (2006).
17. Lynn, F. C. *et al.* MicroRNA expression is required for pancreatic islet cell genesis in the mouse. *Diabetes* **56**, 2938 (2007).
18. Fernández, A. F. *et al.* H3K4me1 marks DNA regions hypomethylated during aging in human stem and differentiated cells. *Genome Res.* **25**, 27–40 (2015).
19. Lee, Y., Jeon, K., Lee, J.-T., Kim, S. & Kim, V. N. MicroRNA maturation: stepwise processing and subcellular localization. *EMBO J.* **21**, 4663–4670 (2002).
20. Dominguez-Gutierrez, G., Xin, Y. & Gromada, J. Heterogeneity of human pancreatic β-cells. *Mol. Metab.* **27S**, S7–S14 (2019).
21. Böni-Schnetzler, M. *et al.* β Cell-Specific Deletion of the IL-1 Receptor Antagonist Impairs β Cell Proliferation and Insulin Secretion. *Cell Rep.* **22**, 1774–1786 (2018).
22. Dror, E. *et al.* Postprandial macrophage-derived IL-1β stimulates insulin, and both synergistically promote glucose disposal and inflammation. *Nat. Immunol.* **18**, 283–292 (2017).
23. Hui, Q. *et al.* Amyloid formation disrupts the balance between interleukin-1β and interleukin-1 receptor antagonist in human islets. *Mol. Metab.* **6**, 833–844 (2017).
24. Meier, C. A. *et al.* IL-1 receptor antagonist serum levels are increased in human obesity: a possible link to the resistance to leptin? *J. Clin. Endocrinol. Metab.* **87**, 1184–1188 (2002).
25. Larsen, C. M. *et al.* Interleukin-1-receptor antagonist in type 2 diabetes mellitus. *N. Engl. J. Med.* **356**, 1517–1526 (2007).
26. Kurtz, C. L. *et al.* MicroRNA-29 fine-tunes the expression of key FOXA2-activated lipid metabolism genes and is dysregulated in animal models of insulin resistance and diabetes. *Diabetes* **63**, 3141–3148 (2014).
27. Xu, H. *et al.* Pancreatic β cell microRNA-26a alleviates type 2 diabetes by improving peripheral insulin sensitivity and preserving β cell function. *PLoS Biol.* **18**, e3000603–e3000603 (2020).
28. Ribeiro, P. V. M., Silva, A., Almeida, A. P., Hermsdorff, H. H. & Alfenas, R. C. Effect of chronic consumption of pistachios (Pistacia vera L.) on glucose metabolism in pre-diabetics and type 2 diabetics: A systematic review. *Crit. Rev. Food Sci. Nutr.* **59**, 1115–1123 (2019).
29. Kanji, M. S., Martin, M. G. & Bhushan, A. Dicer1 is required to repress neuronal fate during endocrine cell maturation. *Diabetes* **62**, 1602–1611 (2013).
30. Thompson, P. J. *et al.* Targeted Elimination of Senescent Beta Cells Prevents Type 1 Diabetes. *Cell Metab.* **29**, 1045-1060.e10 (2019).
31. Aguayo-mazzucato, C. *et al.* Acceleration of b Cell Aging Determines Diabetes and Senolysis Improves Disease Outcomes Article Acceleration of b Cell Aging Determines Diabetes and Senolysis Improves Disease Outcomes. *Cell Metab.* **30**, 129-142.e4 (2019).
32. van Niel, G., D'Angelo, G. & Raposo, G. Shedding light on the cell biology of extracellular vesicles. *Nat. Rev. Mol. Cell Biol.* **19**, 213–228 (2018).
33. Jeppesen, D. K. *et al.* Reassessment of Exosome Composition. *Cell* **177**, 428-445.e18 (2019).
34. Zhang, A. *et al.* Islet β cell: An endocrine cell secreting miRNAs. *Biochem. Biophys. Res. Commun.* **495**, 1648–1654 (2018).
35. Suckale, J. & Solimena, M. The insulin secretory granule as a signaling hub. *Trends Endocrinol. Metab.* **21**, 599–609 (2010).
36. McKenzie, A. J. *et al.* KRAS-MEK Signaling Controls Ago2 Sorting into Exosomes. *Cell Rep.* **15**, 978–987 (2016).
37. Belfiore, A., Frasca, F., Pandini, G., Sciacca, L. & Vigneri, R. Insulin receptor isoforms and insulin receptor/insulin-like

growth factor receptor hybrids in physiology and disease. *Endocr. Rev.* **30**, 586–623 (2009).

38. Wang, J., Gu, W. & Chen, C. Knocking down insulin receptor in pancreatic beta cell lines with lentiviral-small hairpin RNA reduces glucose-stimulated insulin secretion via decreasing the gene expression of insulin, GLUT2 and Pdx1. *Int. J. Mol. Sci.* **19**, (2018).
39. Boucher, J. *et al.* Differential roles of insulin and IGF-1 receptors in adipose tissue development and function. *Diabetes* **65**, 2201–2213 (2016).
40. Lin, H. V & Accili, D. Reconstitution of insulin action in muscle, white adipose tissue, and brain of insulin receptor knock-out mice fails to rescue diabetes. *J. Biol. Chem.* **286**, 9797–9804 (2011).
41. Carey, I. M. *et al.* Risk of Infection in Type 1 and Type 2 Diabetes Compared With the General Population: A Matched Cohort Study. *Diabetes Care* **41**, 513–521 (2018).
42. Moreno-navarrete, J. M. *et al.* Study of lactoferrin gene expression in human and mouse adipose tissue , human preadipocytes and mouse 3T3-L1 fibroblasts . Association with adipogenic and inflammatory markers ☆. *J. Nutr. Biochem.* **24**, 1266–1275 (2013).
43. Zhu, Y. *et al.* MicroRNA-24 promotes pancreatic beta cells toward dedifferentiation to avoid endoplasmic reticulum stress-induced apoptosis. *J. Mol. Cell Biol.* **11**, 747–760 (2019).
44. Li, K. *et al.* Ets1-Mediated Acetylation of FoxO1 Is Critical for Gluconeogenesis Regulation during Feed-Fast Article Ets1-Mediated Acetylation of FoxO1 Is Critical for Gluconeogenesis Regulation during Feed-Fast Cycles. *CellReports* **26**, 2998-3010.e5 (2019).
45. Zhu, Y. *et al.* MicroRNA-24/MODY gene regulatory pathway mediates pancreatic β-cell dysfunction. *Diabetes* **62**, 3194–3206 (2013).
46. Fan, K.-Q. *et al.* Stress-Induced Metabolic Disorder in Peripheral CD4(+) T Cells Leads to Anxiety-like Behavior. *Cell* **179**, 864-879.e19 (2019).
47. Trapnell, C. *et al.* The dynamics and regulators of cell fate decisions are revealed by pseudotemporal ordering of single cells. *Nat. Biotechnol.* **32**, 381–386 (2014).
48. Huang, Q. *et al.* Glucolipotoxicity-Inhibited miR-299-5p Regulates Pancreatic b -Cell Function and Survival. **67**, 2280–2292 (2018).

Acknowledgements

This study was supported by research grants from the National Natural Science Foundation of China (81870531 and 81670703 Y-X.Z.; 81830024 to X.H.). X.H. and Y.X. are fellows at the Collaborative Innovation Center for Cardiovascular Disease Translational Medicine.

Author contributions

Conceptualization, X.H., and Y-X.Z.; Methodology, Y-C.Z., K-R.L., Y.S., Y.Z., Y.W., and P.S.; Formal Analysis, X.H., Y-X.Z., and Y-C.Z.; Investigation, Y-X.Z., Y-C.Z., K-R.L., Y.S., Y.Z., and Y.W.; Resources, S.W., W.T., Y.L., R.B., R.L., and X.C.; Writing - Original Draft, Y-X.Z., Y-C.Z. and K-R.L.; Writing – Review & Editing, X.H. and Y-X.Z.; Visualization, Y-C.Z., and Y-X.Z.; Supervision, X.H., and Y-X.Z.; Funding Acquisition, X.H., and Y-X.Z. All authors reviewed and commended on the manuscript.

Competing interests

The authors declare no competing interests.

Additional information

Supplemental Information includes figures and tables and can be found with this article.

Reprints and permission information is available online at http://npg.nature.com/reprintsandpermissions/

Figures

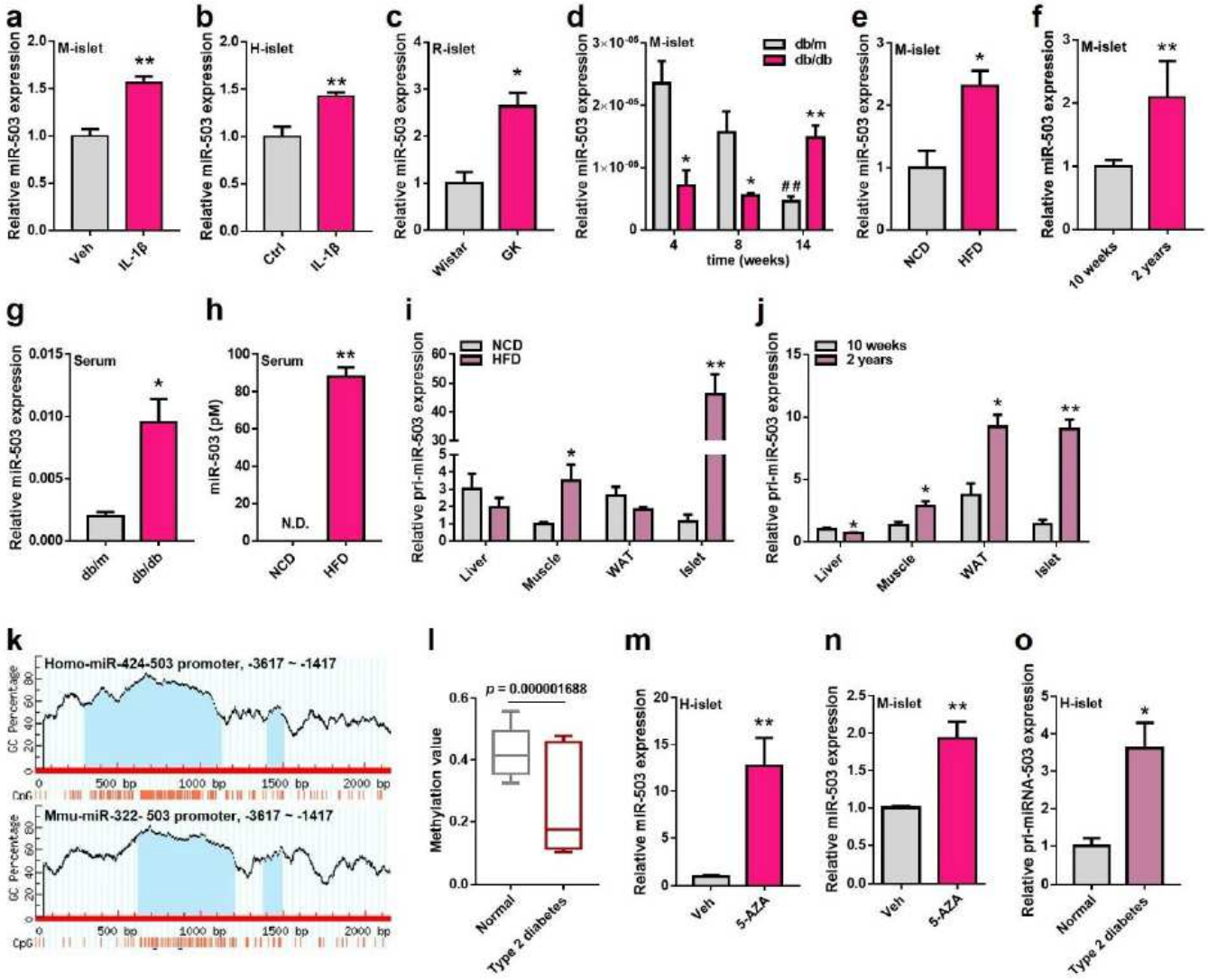

Figure 1

Promoter hypomethylation permits miR-503 expression in β cells under inflammation and diabetes conditions. a, b MiR-503 expression in primary islets treated with 10 ng/ml IL-1β for 24 h was measured by qPCR: mice (a) or human (b) islets. c-f qPCR assays showing miR-503 expression in diabetic murine islets: GK rats (c), different aged db/db mice (d), 4-month HFD fed C57/BL6J mice (e), 2-year-old C57/BL6J mice (f). g, h MiR-503 contents in mice serum by using relative qPCR assay in 14-week-old db/db mice (g) or by absolute qPCR assay in 4-month HFD fed C57/BL6J mice (h). i, j qPCR analysis of miR-503 transcription level represented by pri-miR-503 expression of 4-month HFD fed (i) and 2-year-old C57/BL6J mice (j) tissue. k CpG island analysis of miR-503HG promoter region separately in human (up) and mice (down) by using MethPrimer program. l DNA methylation analysis of miR-503HG promoter in T2D patients in accordance with DiseaseMeth database. m, n Human (m) and mice (n) islets were treated with 10 μmol/l 5-AZA for 24 h, and miR-503 expression was quantified by using qPCR assay. o qPCR

analysis of miR-503 transcription level represented by pri-miR-503 expression in islets from healthy or T2D patients. Bar graph data are presented as mean ±SEM, *p < 0.05, **p < 0.01, t test, n ≥ 3 per group.

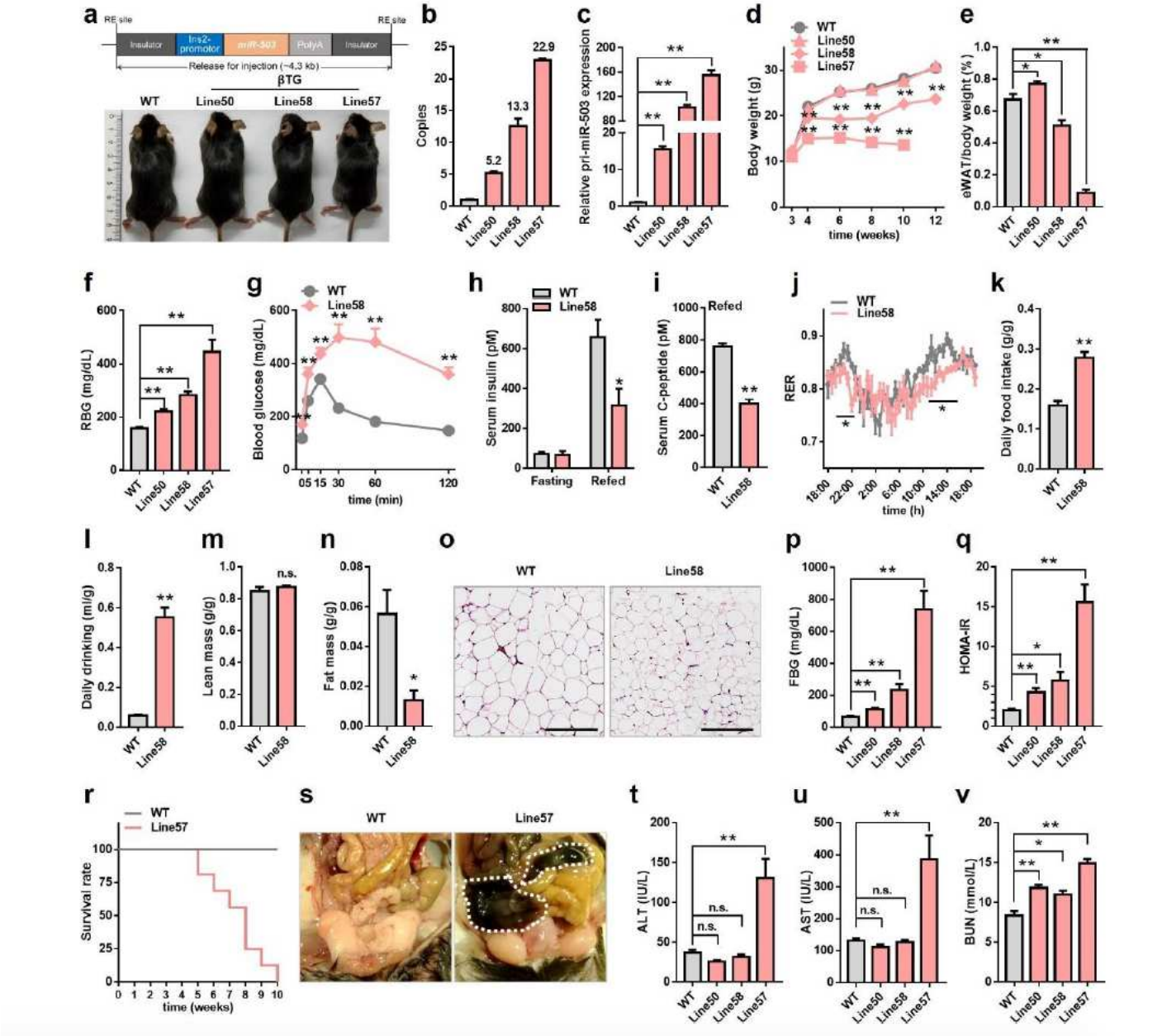

Figure 2

β-cell transgenic overexpressed miR-503 promotes diabetes and lethality. a The schematic of recombinant plasmid used for β cell specific transgenic miR-503 mice construction and whole-mount image. b-f Gene copies (b), miR-503 expression (c), body weight accompanies with age (d), percentage of white adipose tissue in body weight (e), and plasma glucose level of randomly fed three βTG line mice and their littermates (f). g-i IPGTT (g), serum insulin (h) and c-peptide (i) level of 6-week-old Line58 mice. j-o Daily respiratory exchange rate (j), daily food intake (k), daily drinking (l), lean mass (m), fat mass (n) and adipose tissue section (o) of 10-week-old Line58 mice and their littermates. p, q Fasted blood glucose and HOMA-IR of 6-week-old three βTG line mice and their littermates. r ,s Survival rate (r) and lower abdomen image (s) of Line57 and WT mice. (t-v) Glutamic-pyruvic transaminase (t), glutamic oxalacetic

transaminase (u), and blood urea nitrogen (v) level in 10-week-old mice serum. Error bars represent the SEM, N.S. means not significant, *p < 0.05, **p < 0.01, t test, n ≥ 3 per group.

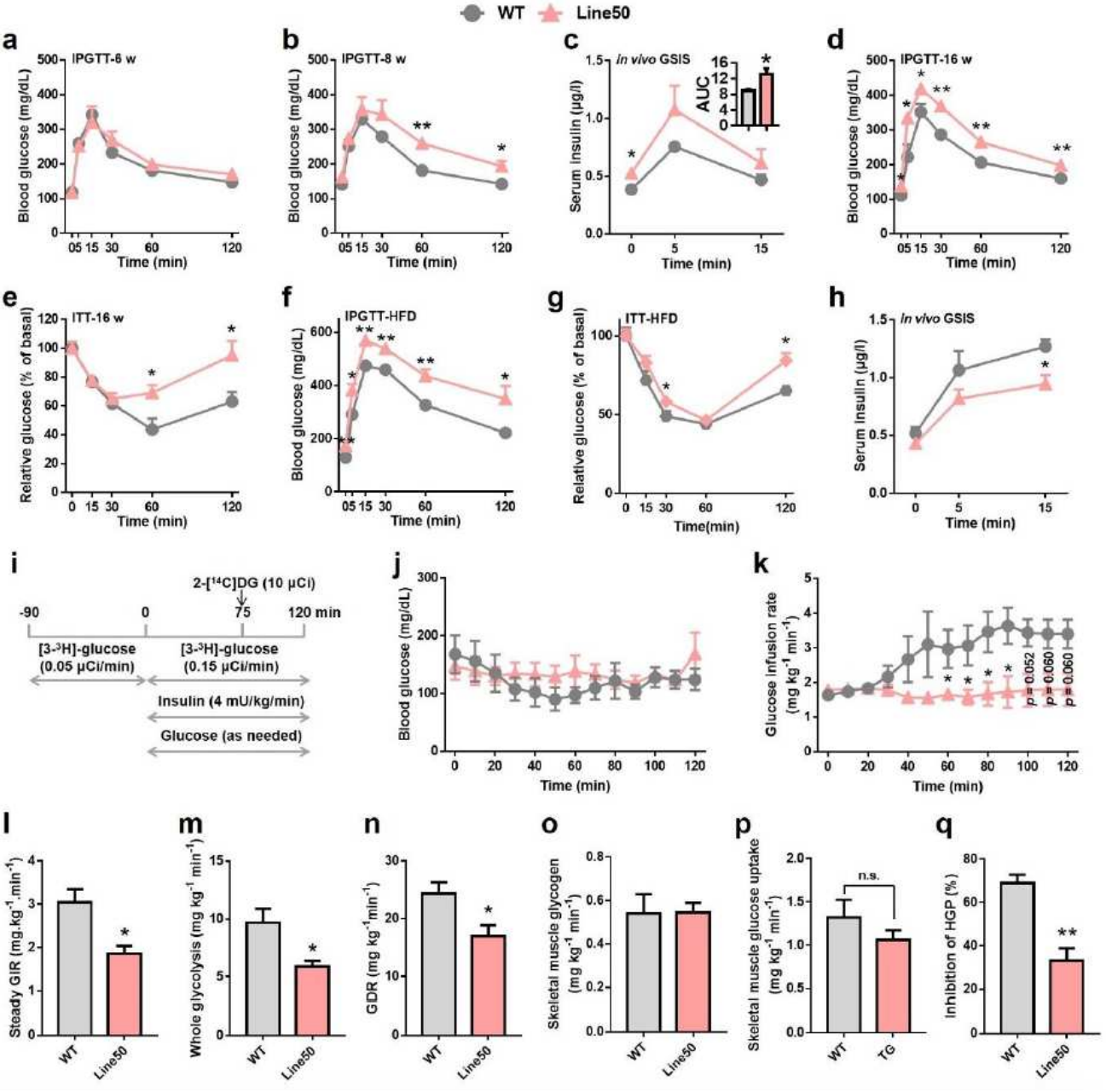

Figure 3

Metabolic stress enhances miR-503 induced insulin resistance and glucose intolerance. a-e IPGTT (a, b and d), in vivo GSIS (c), IPITT (e) of randomly fed Line50 mice and their littermates. Mice at the age of 6 weeks(a), 8 weeks (b, c), 16 weeks (d, e). f-h IPGTT (f), IPITT (g), and in vivo GSIS (h) of 2-month HFD fed Line50 and WT mice. i-q Hyperinsulinemic-euglycemic clamp assay of 16-week-old WT and Line50 mice, protocol (i), blood glucose levels (j), glucose infusion rate (k), statistical analysis of GIR (l), whole body glycolysis (m), rate of glucose disposal (n), adipose tissue glucose uptake (o), skeletal muscle glucose uptake (p) and inhibition of hepatic glucose production (q). Error bars represent the SEM, *p < 0.05, **p < 0.01, t test, n ≥ 3 per group.

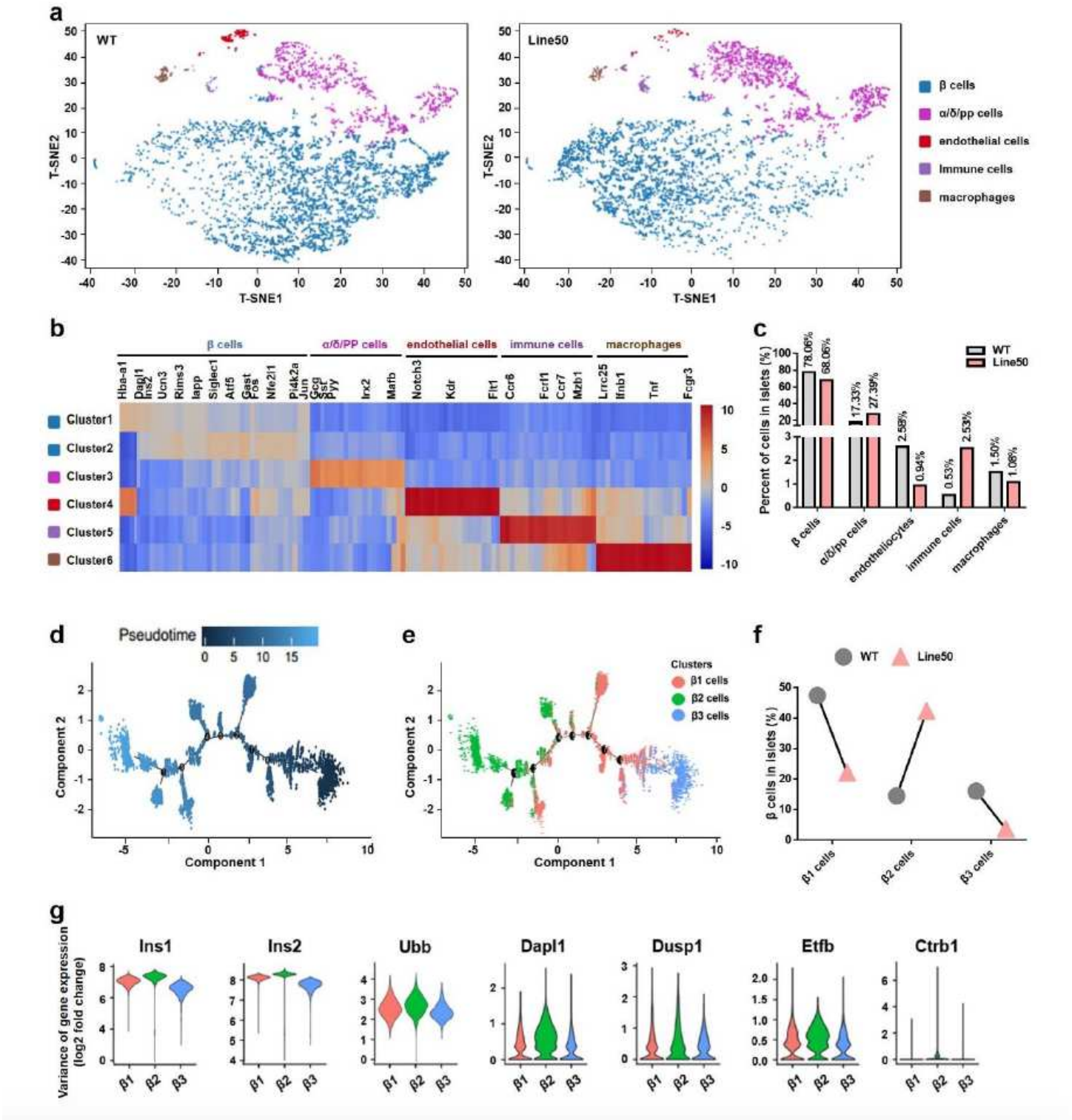

Figure 4

ScRNA-Seq Identifies Immune-Cell Infiltration and β-Cell Senescence in miR-503TG islets. a-g Analysis of scRNA-sequence of islets from 10-week-old WT and Line50 mice, tSNE plots (a), heatmap of all cells clustered by K-means = 5 clustering, showing selected marker genes for every population (b), percentage of each cell clusters in islets from WT or Line50 mice separately (c), maturation trajectory (d) and distribution (e) of three subtype β cells constructed by Monocle, percentage of different subtype β cells

from different mice respectively (f), specific senescence associated genes across sub-clusters demonstrated by violin plots (g). Cell types are represented by colors.

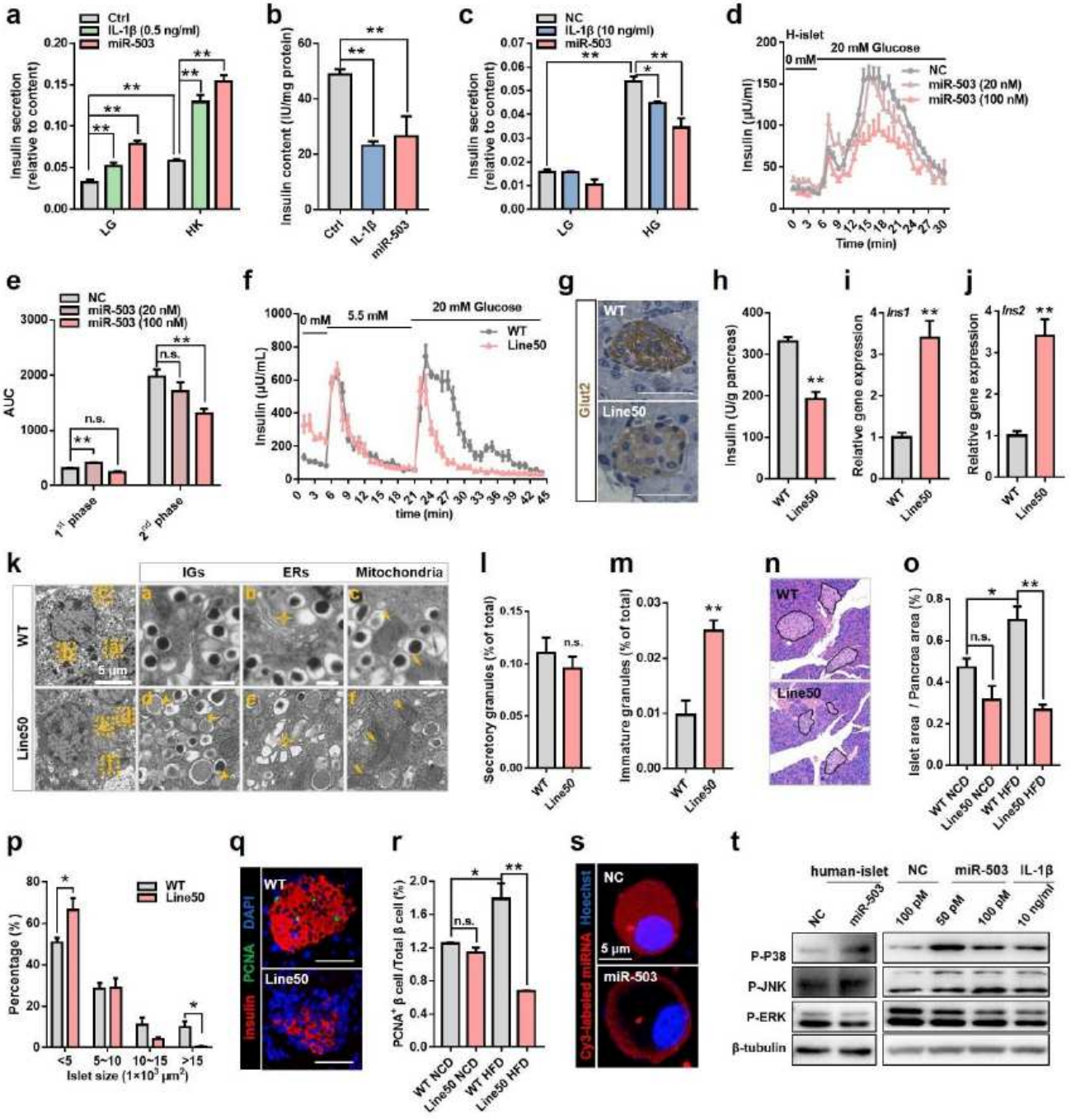

Figure 5

miR-503, Akin to IL-1β Causes β-Cell Defect via Activating MAPK and NF-κB Pathway. a-e Cells or primary human islets transfected with NC or miR-503 mimics for 48h, then insulin secretion and content were assessed by KSIS, GSIS or islets infusion. KSIS (a) and content (b) of INS-1 cells, GSIS of MIN6 cells (c), islet perfusion (d) and area under curve (AUC) the first and second phases (e) of primary human islets. f Islets infusion of 10-week-old WT and Line50 mice islets. g-j Representative images of Glut2 immunohistochemical staining of pancreatic sections (g), the white bars refer to 200 μm, insulin content

of pancreas standardized by weight (h), insulin gene expression in islets (i, j) from 10-week-old WT or Line50 mice. k-m Transmission electron microscopic (TEM) images of the pancreatic islets where orange arrows or stars point to IGs in d, endoplasmic reticulum in b and e, mitochondrial in c and f (k), and statistical results of secretory insulin granule (l) and ISG (m), islets were isolated from 10-week-old Line50 mice and their littermates. n Pancreas section from 10-week-old randomly fed mice stained by hematoxylin and eosin (H & E stain). o Islet mass represented by area amount percentage of pancreas, and statistical analysis results of islet mass from both NCD and 2-month HFD fed WT or Line50 mice. p-r Reasons for islet mass decrease, 10-week-old NCD mice islet size distribution (p) and PCNA staining of pancreas section represent for evaluation of replication rate (q). s Primary β cells from 8-week-old male C57BL/6J mice were transfected with Cy3 labeled duplex NC and miR-503 mimics before which adenovirus were added to media for 1hr. t Immunoblot analysis of phospho-p38, phospho-JNK and phosphor-ERK in primary human islets or MIN6 cells transfected with NC or miR-503 mimics for 48 h. Error bars represent the SEM, N.S. means not significant, *p < 0.05, **p < 0.01, t test, n ≥ 3 per group, TEM and WB were repeated three times.

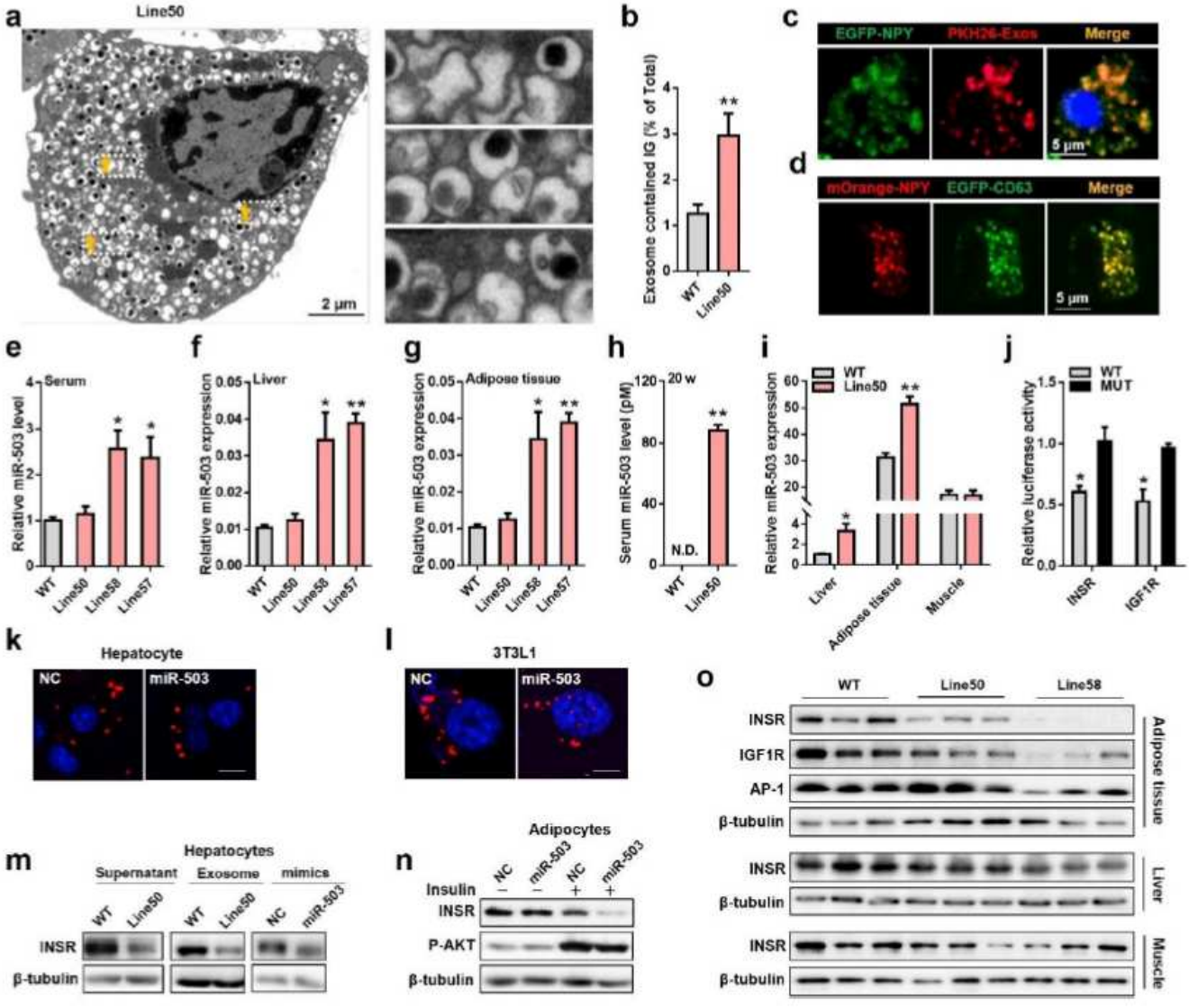

Figure 6

Beta-Cell Derived miR-503 Targets Insr to Inhibit Insulin Action in Liver and Adipose Tissue. (a, b) TEM photograph (a) of β cell from 10-week-old Line50 mice where orange arrows indicate exosome contained IGs and the statistical result (b). (c, d) Representative images for insulin granule and exosome co-localization, primary β cells from 8-week-old C57BL/6J mice islets transfected with EGFP-NPY adenovirus for 12 h, and PKH26 stained exosomes which extracted from 16-week-old Line50 mice islets were added into media for 8 h (c), MIN6 cells co-transfected with mOrange-NPY adenovirus and EGFP-CD63 plasmid for 12 h (d). e-g MiR-503 expression in serum (e), liver (f) and white adipose tissue (g) from 8-week-old βTG mice and their littermates. h, i MiR-503 content in serum (h) or miR-503 expression in tissues (i) from 16-week-old WT or Line50 mice. j Luciferase reporter assay was carried out 24h after 293T cells co-transfected with wt or mut reporter plasmids, PRL-SV40 plasmid and NC, or miR-503. k, l Images of primary hepatocyte (k) or mature adipocyte differentiated from 3T3L1 cells (l) transfected for cy3 labeled NC or miR-503 mimics, the white bar refers to 50 μm. m Immunoblot analysis of INSR expression in primary hepatocytes treated with islets supernatant and exosomes extracted from 16-week-old WT or Line50 mice islets, or NC and miR-503 mimics for 48 h. n Immunoblot analysis of INSR and p-AKT expression in mature adipocyte transfected with NC or miR-503 mimics for 48h, before the sample collection 100 nmol/l insulin or physiological saline was added in media for 10 min. o Immunoblot analysis of INSR and IGF1R expression in adipose tissue, liver, and skeletal muscle from 8-week-old WT, Line50 and Line58 mice. Error bars represent the SEM, *$p < 0.05$, **$p < 0.01$, t test, $n \geq 3$ per group, immunofluorescence and WB were repeated three times.

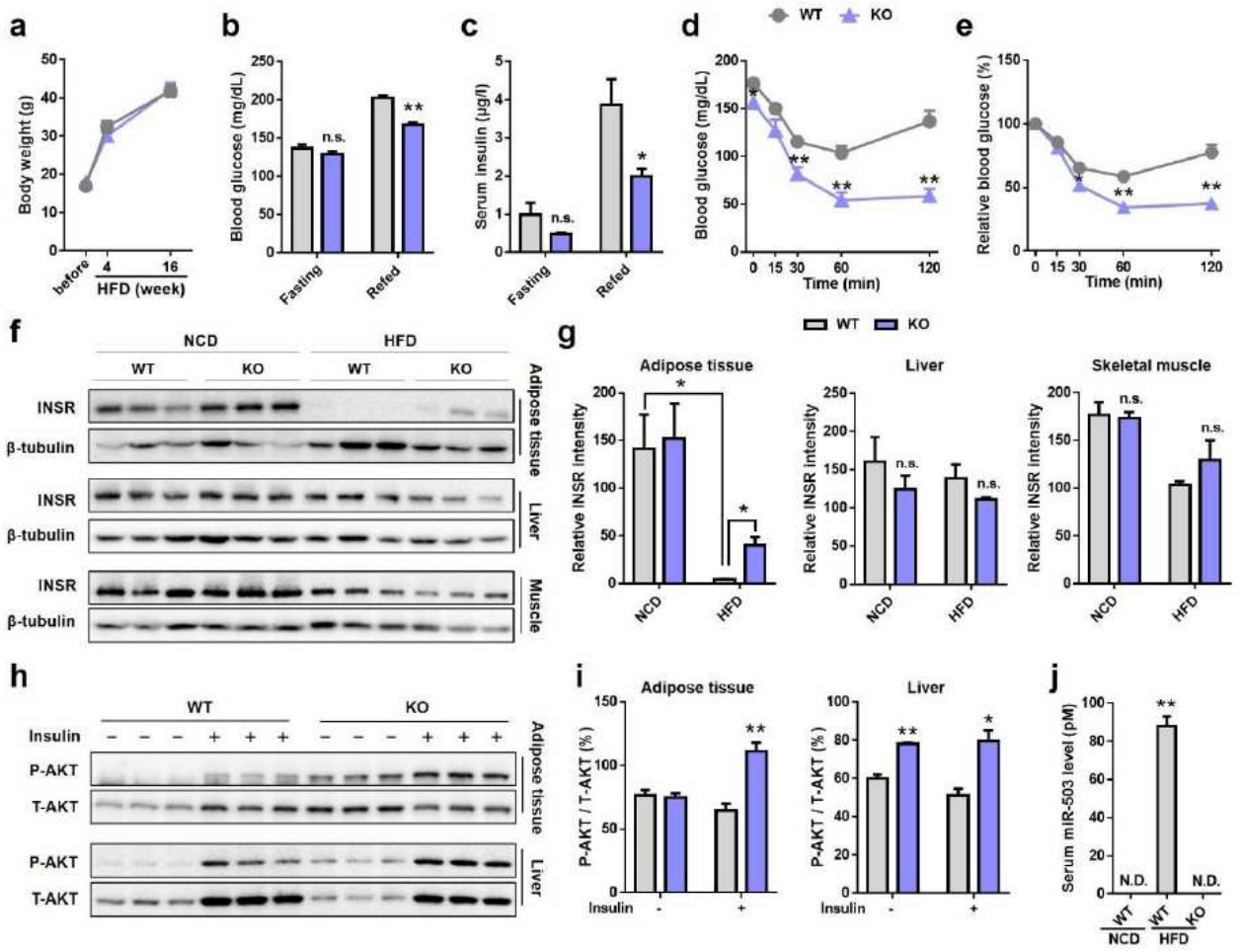

Figure 7

Deletion of miR-503 Cluster Ameliorates HFD Induced Insulin Resistance in Mice. a Body weight of HFD fed WT or KO mice in accompany with age. b-e 16hrs fasted and 2hrs after meal blood glucose test (b) and serum insulin level (c), IPITT (d) and standardized IPITT (e) of 4-month HFD fed WT and KO mice. f, g Immuno-blot analysis of INSR expression (f) in WAT, liver and skeletal muscle and their gray analysis (g). h, i 4-month HFD WT and KO mice liver, adipose tissue and skeletal muscle phosphor-AKT and AKT protein expression with or without insulin injection were performed using western blotting (h) and their gray analysis (i). j MiR-503 contents in mice serum. Error bars represent the SEM, N.D. refers to not detected, *p < 0.05, **p < 0.01, t test, n ≥ 3 per group.

Supplementary Files

This is a list of supplementary files associated with this preprint. Click to download.

- SupplementaryinformationexosomalmiR503.pdf